5-2016

Structural and Biochemical Characterization of the Frequency-Interacting RNA Helicase FRH

Jacqueline M. Johnson
Utah State University

STRUCTURAL AND BIOCHEMICAL CHARACTERIZATION OF THE FREQUENCY-INTERACTING RNA HELICASE FRH

by

Jacqueline M. Johnson

A thesis submitted in partial fulfillment
of the requirements for the degree

of

MASTER OF SCIENCE

in

Biochemistry

Approved:

_____	_____
Dr. Sean J. Johnson Major Professor	Dr. Joan M. Hevel Committee Member
_____	_____
Dr. Nicholas E. Dickenson Committee Member	Dr. Mark R. McLellan Vice President for Research and Dean of the School of Graduate Studies

UTAH STATE UNIVERSITY
Logan, Utah

2016

ABSTRACT

Structural and Biochemical Characterization of the

Frequency-interacting RNA Helicase

by

Jacqueline M. Johnson, Master of Science

Utah State University, 2016

Major Professor: Dr. Sean J. Johnson
Department: Chemistry and Biochemistry

RNA is a molecular messenger of the cell, essential to many cellular pathways and processes. In order to maintain functionality, RNA is processed and modified by protein complexes such as the exosome and associated proteins. The exosome-mediated RNA processing or degradation both require a Ski-2 like helicase to function. One such helicase is the Frequency-interacting RNA Helicase (FRH), an essential RNA helicase from *Neurospora Crassa*. FRH is homologous to the *Saccharomyces cerevisiae* Mtr4 from the Ski2-like family of RNA helicases. Sequence alignments between FRH and Ski2-like family helicases predicted FRH to share the helicase core domains and the inserted arch domain a characteristic of the Mtr4-like proteins in this protein family. FRH is also a main component of the circadian oscillation pathway in *N. crassa*. The participation of FRH in

circadian oscillation is not a shared role across RNA helicases. FRH forms a link between two major cellular pathways providing a unique system to study RNA surveillance. Here we present the 3.51Å and 3.25Å crystal structures of FRH which supports structural prediction by maintaining the core architecture found in Ski2-like helicases. These similarities are accompanied by significant flexibility of the arch domain and revealed a unique homodimer. Other known Ski2-like helicases have not been observed to form dimers and function biologically as monomers. Furthermore, the initial characterization of helicase activity of FRH on a poly-adenylated RNA substrate is presented. Also explored is the evidence of a dimer through crosslinking and size exclusion chromatography assays.

(83 pages)

PUBLIC ABSTRACT

Structural Characterization of FRH

A Dual Functioning RNA Helicase

by

Jacqueline M Johnson, Master of Science

Utah State University, 2016

Major Professor: Dr. Sean J. Johnson
Department: Chemistry and Biochemistry

Cells function through a variety of regulatory pathways intricately communicating with one another. These pathways ensure that cellular functions happen at the appropriate times and keep the natural balance within the cell. When pathways do not communicate appropriately, this can lead to disease states and cell death. Two such connected pathways in *Neurospora crassa* involve the regulation of RNA levels and the circadian rhythms essential for these cells to maintain homeostasis. These pathways are connected by a unique helicase called the Frequency-interacting RNA Helicase (FRH), named for its discovery with the frequency protein involved in the circadian oscillation of the fungus, *N. crassa*. All eukaryotes require a way to maintain RNA levels within the cell, in eukaryotes the majority of RNA is processed or degraded by the exosome and associated proteins. The exosome requires an RNA helicase from the family of Ski2-like helicases to function. In *N. crassa* this Ski-2 like helicase is FRH. Other RNA helicases have been studied,

especially in yeast with the similar protein Mtr4 that is also involved in RNA surveillance. Due to this similarity it is predicted that FRH has a similar structure and function to Mtr4. However, no other RNA helicase has been shown to be incorporated in the separate regulation of circadian rhythms. The role of FRH in *Neurospora* is intriguing and provides a unique system to study both RNA surveillance and circadian oscillation. Here we present a structural and biochemical characterization of FRH which is similar to the yeast Mtr4 yet forms a unique dimer not previously observed. Discussion for the biological relevance of the FRH dimer is presented and future work proposed.

Jacqueline M. Johnson

ACKNOWLEDGMENTS

I would especially like to thank my amazing Principle Investigator Dr. Sean J. Johnson for constant support, guidance, and wisdom. Without Dr. Johnson's encouragement, I would have never succeeded. I would also like to acknowledge Dr. Joan M. Hevel, for encouraging me to continue through all the road blocks graduate school entails. Furthermore, I would like to thank my committee members Dr. Joan M. Hevel and Dr. Nicholas E. Dickenson for scientific discussion, troubleshooting, and equipment utilized for this research. To my coworker, Yalemi Morales, I would like to thank her for help with designing and performing experiments crucial in demonstrating the significance of this work. Yalemi's leadership and perseverance have been a constant example for my own scientific goals. Lastly, I give special thanks to my fiancé Marc Bulcher, for his unwavering support and many comfort food meals provided throughout the entire process.

Jacqueline M. Johnson

CONTENTS

LIST OF TABLES

LIST OF FIGURES

CHAPTER 1

BACKGROUND AND SIGNIFICANCE

OVERVIEW

RNA is a molecular messenger used by cells to transcribe genetic information from DNA, perform catalytic functions, and respond to cellular needs. RNA is under constant cellular surveillance including modification, localization and degradation. The exosome and associated proteins are one of the major RNA modification, surveillance, and degradation complexes within the cell (Allmang et al., 1999). The exosome complex (EC) deals with all types of RNA in processes including, stabilizing RNA through 3' end maturation, degrading fragments of RNA resulting from processing or unstable transcripts, and quality control (Schneider and Tollervey, 2013) (Chlebowskia et al., 2013). Malfunctions in the exosome machinery have been linked to autoimmune and human mendelian diseases (Fabre and Badens, 2014) . In order for the exosome to function, activation by a Ski2-like RNA helicase is essential (Jacobs Anderson and Parker, 1998; Liang et al., 1996). In the nucleus, this essential helicase is Mtr4, a 3'-5' RNA helicase (Liang et al., 1996). Mtr4 is found in many eukaryotic species including plants, fungi, and humans in various complexes that function to bring RNA to the exosome for processing or degradation (Johnson and Jackson, 2013). The most characterized Mtr4 complex is the eukaryotic TRAMP complex used for the processing and degradation of RNA. In yeast, the TRAMP (Trf4/Air2/Mtr4pPolyadenylation) complex contains an RNA helicase

(scMtr4), a poly-A polymerase (Trf4 or Trf5), and a zinc knuckle protein (Air1 or Air2) (Vanacova et al., 2005). Air1 or Air2 is thought to recruit RNA substrates to the complex, then Trf4 of Trf5 adds a short poly-A tail to the RNA substrate, which can then be unwound by the Mtr4 helicase and delivered to the exosome for processing or degradation (Vanacova et al., 2005). Another substrate targeting route, uncovered in yeast, involves a specific interaction with the arch domain of Mtr4 through an arch interacting motif (AIM) to recruit Mtr4 to diverse RNA substrates for modification as well as degradation (Thom et al., 2015). Many of these proteins involved in an Mtr4 complex are homologous to human proteins and can be found across the eukaryotic kingdom (Johnson and Jackson, 2013). With a variety of model systems to study RNA surveillance available, *Neurospora* provides a unique well-defined model organism. Herein, the model system used is *Neurospora crassa,* where RNA surveillance is linked to the circadian oscillation pathway through the use of an Mtr4 helicase homolog in both pathways (Guo et al., 2009).

N. crassa, contains an Mtr4-like protein named the frequency-interacting RNA helicase, or FRH (Cheng et al., 2005). FRH was first identified within the circadian oscillation pathway of the fungus and is 55% identical and 73% similar in amino acid sequence to the Mtr4 protein observed in *S. cerevisiae* (Cheng et al., 2005). Aside from being identified as an Mtr4-like RNA helicase, FRH also functions in the circadian oscillation pathway, traversing both the cytosol and the nucleus (Guo et al., 2009). In the oscillation pathway, FRH functions as a negative regulator of clock controlled genes through repressing the transcription up-regulator white collar complex (WCC) (Cheng et al., 2005). This regulatory role is accomplished through an association with the intrinsically disordered frequency protein, FRQ (Hurley et al., 2013). Extensive research

has focused on FRQ interactions to understand the mechanisms of circadian oscillation (Guo et al., 2010); however, the FRH helicase has not been studied in the context of RNA regulation pathways. Currently, little enzymatic characterization and no structural information has been uncovered to understand the essential role FRH plays in both the circadian oscillation and the RNA surveillance pathways. Presented in this work is a literature background followed by the structural and biochemical characterization of FRH.

RNA 3'END MODIFICATIONS

RNA provides the cell with a variety of roles from a molecular messenger, to a protein code, and catalytic activities. RNA regulates essential cellular pathways including transcription and translation however, most types of RNA need to be processed or modified to become active (Allmang et al., 1999). Common modifications include 5' capping, 3' end poly-adenylation (poly-A), splicing, trimming, and covalent modifications (Allmang et al., 1999; Mitchell, 2014; Viegas et al., 2015). Modifications of the 3' end effect stability, localization, and functions of RNAs (Mitchell, 2014). Specifically, the addition of a long poly-A tail to the 3' end has been shown to stabilize RNA transcripts and promotes cellular transport from the nucleus to the cytosol (Viegas et al., 2015). Usually, the long poly-A tail is accompanied by a 5' cap on the RNA, also to prevent degradation (Bernstein and Toth, 2012). Shortening of the poly-A tail can destabilize the RNA transcripts and signal for degradation in the cytosol (Viegas et al., 2015). Furthermore, addition of a short poly-A tail on the 3' end by the TRAMP complex can be a signal for processing or degradation of RNA with the nuclear EC (Figure 1-1) (Vanacova et al., 2005). The nuclear exosome and significance of exosome-mediated RNA degradation is discussed in the following section.

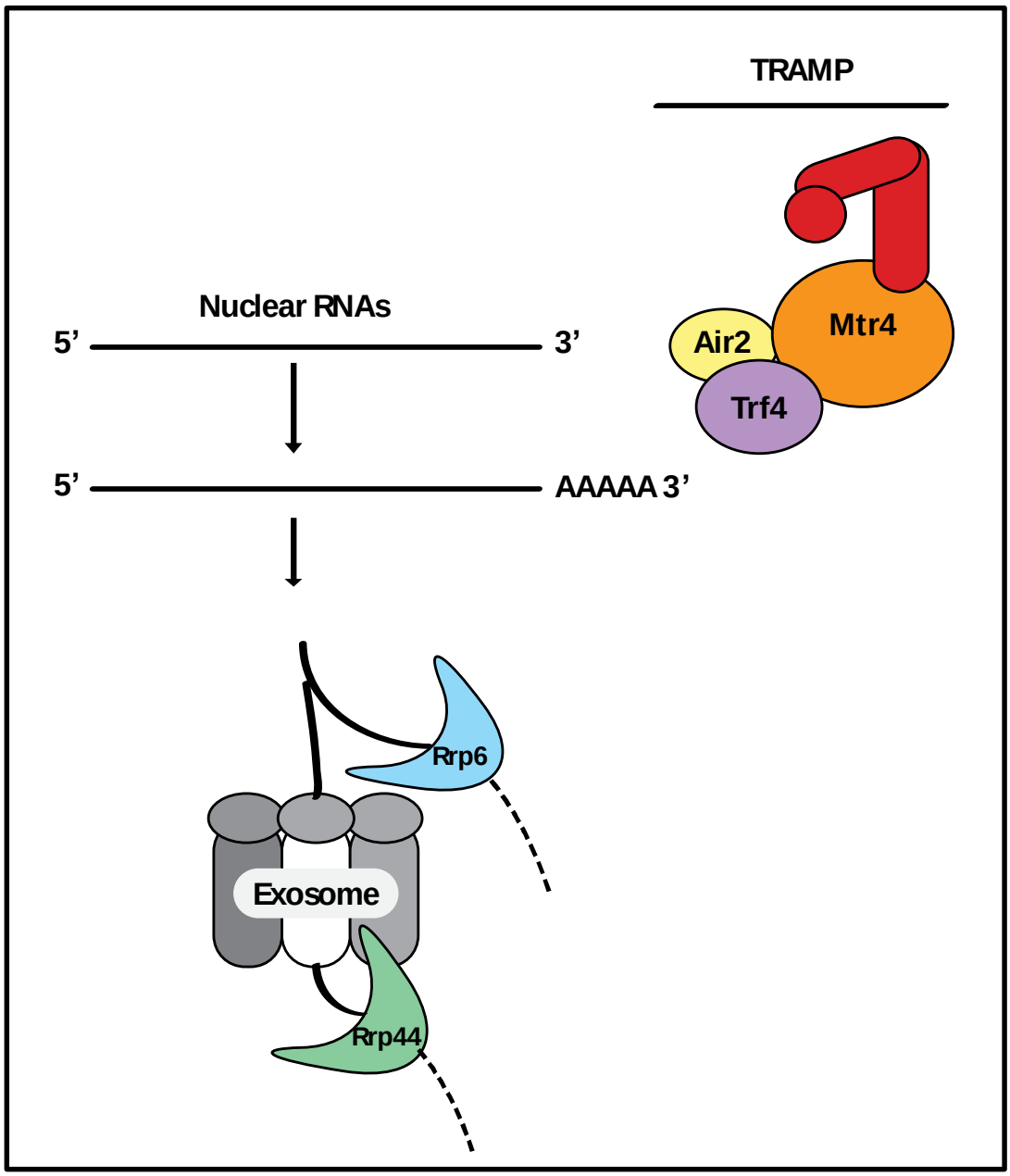

Figure 1-1. Eukaryotic Exosome-Mediated RNA Degradation. A schematic of the nuclear TRAMP complex shown above (Mtr4 core (orange), Mtr4 arch (red), Trf4 (purple), Air2 (yellow)) adenylates nuclear RNAs before presenting unwound RNA to the exosome complex (grey) for degradation through the ribonucleases Rrp6 (blue) and Rrp44 (green) (Taylor, 2014).

THE EXOSOME FUNCTIONS IN RNA DEGRADATION AND SURVEILLANCE

The exosome is one of the main components of RNA degradation and surveillance (Jacobs Anderson and Parker, 1998). Composed of a barrel-like structure formed from two stacked rings of RNA binding proteins, the eukaryotic exosome alone has no catalytic function (Liu et al., 2006). The exosome core associates with two ribonucleases to degrade ssRNA at the top (Rrp6) (Cristodero et al., 2008) and bottom (Rrp44) (Wang et al., 2007) of the core where the RNA is threaded through (Mitchell et al., 1997). For the nuclear exosome complex to receive the ssRNA, the 3'-5' RNA helicase Mtr4 is essential (Vanacova et al., 2005) (Figure 1-1). In the nucleus, the exosome has been shown to process precursor RNAs including rRNA, snoRNA, snRNA, and the by-products of these reactions (Allmang et al., 1999; Schneider and Tollervey, 2013). In surveillance, the nuclear exosome also receives many cryptic unstable transcripts (CUTs) (Wyers et al., 2005). The process by which substrates are recruited to the exosome is not well understood.

In some cases, the associated proteins in the TRAMP complex are required for exosome-mediated RNA degradation (Vanacova et al., 2005; Wyers et al., 2005). The TRAMP complex contains an RNA helicase (Mtr4), a poly-A polymerase (Trf4 of Trf5), and a zinc knuckle protein (Air1 or Air2) (Vanacova et al., 2005). Air1 or Air2 are thought to recruit RNA substrates to the complex where Trf4 or Trf5 poly-adenylates the RNA substrates (Vanacova et al., 2005). Mtr4 then presumably unwinds the secondary structure of the RNA providing the EC with a linear substrate for processing or degradation (Bernstein et al., 2008). It has been demonstrated that in the presence of ATP RNA substrates with a poly-A tail are the preferred substrate of the RNA helicase Mtr4 (Bernstein et al., 2008). The Mtr4 helicase is an essential partner for the nuclear exosome

thought to provide necessary momentum by unwinding RNA substrates (Bernstein et al., 2008) (Figure 1-1). TRAMP is not the only Mtr4-complex involved in processing RNA substrates, in fact a different substrate recruitment mechanism for other types of RNAs has recently been investigated (Thom et al., 2015).

This substrate recruitment mechanism utilizes an interaction in the Mtr4 arch through an arch interacting motif (AIM) (Thom et al., 2015). The AIM motif was found in the yeast Nop53, a homolog of the human tumor suppressor protein PICT1, as well as the yeast Utp18 protein, an essential subunit of the 90S pre-ribosome (Thom et al., 2015). Nop53 recruits Mtr4 to pre-ribosomal RNA for processing by the exosome, while Utp18 recruits Mtr4 to rRNA fragments for exosome-mediated degradation (Thom et al., 2015). This recruitment process utilizes the same AIM interaction to recruit Mtr4 to different types of substrates through a general mechanism that may be conserved throughout eukaryotes with evidence of these proteins in various species (Thom et al., 2015). Some of these species include; *Schizosaccharomyces pombe, Kluyveromyces lactis, Neurospora crassa, Drosophila melanogaster, Mus musculus,* and *Homo sapiens* (Thom et al., 2015). The AIM recruitment pathway is an example of how specific RNA substrates are targeted and processed by the exosome and could lead to further understanding of how other RNA substrates are identified. Processing and turnover of RNA is vital to the cell and it is important to remember that none of these substrates would reach the nuclear exosome without a Ski2-like RNA helicase (Jacobs Anderson and Parker, 1998).

Mtr4

Mtr4 is a Ski2-like 3'-5' helicase from the superfamily 2 (SF2) of helicases (Fairman-Williams et al., 2010). Ski2-like helicases include both DNA and RNA helicases (Johnson and Jackson, 2013). Specifically, Ski2-like RNA helicases are Ski2, Mtr4, Brr2, and S1h1 (Johnson and Jackson, 2013). Classification of these families are based on common sequence, structural, and mechanistic features to distinguish them from other protein families (Fairman-Williams et al., 2010). One of these classifying features includes the two RecA-like domains shared by superfamily 1 and superfamily 2 helicases (blue and yellow Figure 1-2) (Fairman-Williams et al., 2010). These domains are responsible for ATP hydrolysis and nucleotide interactions that form the helicase core (Fairman-Williams et al., 2010; Johnson and Jackson, 2013). The helicase core forms a circular pore with two other domains in Ski2-like helicases named the winged helix and ratchet helix (sometimes referred to as the helical domain) (green and purple Figure 1-2) (Fairman-Williams et al., 2010; Johnson and Jackson, 2013). The winged helix is a small domain while the ratchet helix consists of a seven helical bundle first observed in the SF2 DNA helicase Hel308 structure (Buttner et al., 2007). The first crystal structure of *Saccharomyces cerevisiae* Mtr4 (scMtr4) was solved in 2010 by the Johnson lab (Figure 1-2A-B, PDB ID 4QU4) (Jackson et al., 2010). The scMtr4 structure revealed a novel arch domain inserted into the winged helix observed in other SF2 helicases (Jackson et al., 2010). The arch domain is unique to Ski2 and Mtr4 helicases (Johnson and Jackson, 2013). In Mtr4, sometimes the arch is referred to as the KOW domain due to the first portion of the arch containing a KOW motif (Weir et al., 2010). Two other structures of scMtr4 have since been solved (Falk et al., 2014; Weir et al., 2010), one containing ADP and a five nucleotide long single

stranded RNA substrate (PDB ID: 2XGJ) and another with peptides of TRAMP components Air2 and Trf4 (PDB ID: 4U4C). A similarity between all of the scMtr4 structures is that the N-terminal region is missing from them possibly due to the region predicted to be unstructured through secondary structure analysis (Jones, 1999). Despite the structural information on scMtr4, little is known about the functional role of the arch domain. Investigation of the arch domain has revealed that the arch can bind to structured RNAs and may be involved in RNA processing (Taylor et al., 2014). Another study has uncovered the AIM motif found in *S. cerevisiae* Nop53 and UTP18 used to recruit scMtr4 to the exosome (Thom et al., 2015). The AIM motif interaction is only one example of Mtr4 in a vast number of protein complexes formed for RNA surveillance across eukaryotes. Mtr4 has been identified in eukaryotic complexes from *S. cerevisiae, S. pombe, H. sapiens, N. crassa*, and possibly others that have been linked to exosome-mediated degradation (Johnson and Jackson, 2013). In an effort to elucidate the roles of the arch domain and interacting proteins in RNA surveillance and decay, studying these Mtr4 homologs and complexes becomes necessary. One such interesting Mtr4 homolog from *Neurospora crassa* is the Frequency-interacting RNA helicase (FRH) (Cheng et al., 2005).

FRH is predicted to be similar to scMtr4 both structurally and functionally. Based on amino acid sequence alignments, FRH is 55% identical and 73% similar to scMtr4 with highly dissimilar regions found in the disordered N-termini (Altschul et al., 1997) (Figure 1-3). Although there is high similarity in primary sequence between the two helicases, the enzymatic activity of FRH has not been characterized. FRH has also been shown to be associated with the catalytic exosome subunit Rrp44 in *N. crassa* (Guo et al., 2009).

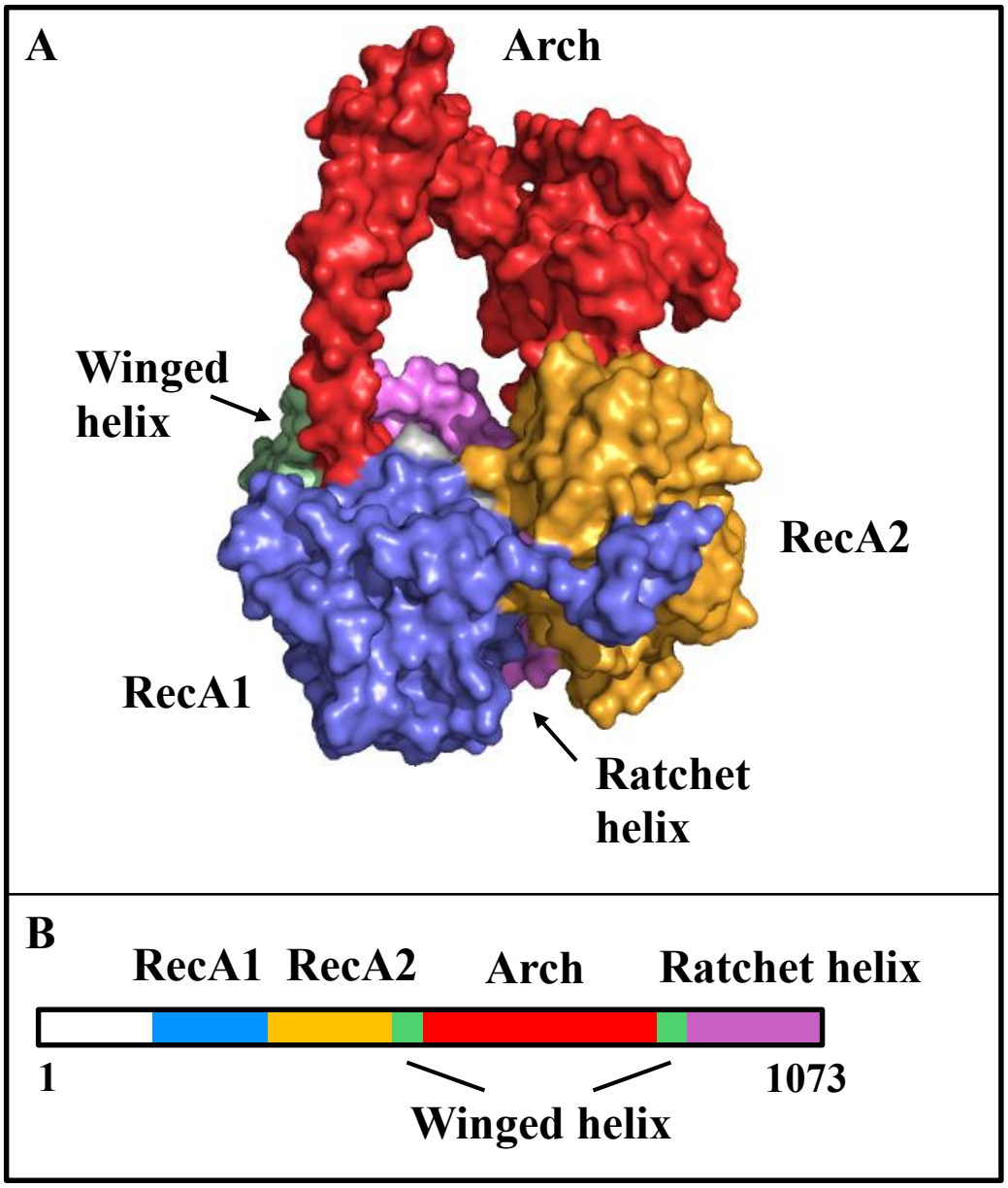

Figure 1-2. Mtr4 Domains. A- scMtr4 is shown above in a surface depiction (PDB ID: 4QU4) (PyMol) with domains colored blue (RecA1), yellow (RecA2), green (winged helix), red (arch), and magenta (ratchet helix). **B**- Sequence of scMtr4 color coded as in 2A.

Furthermore, BLAST searches of TRAMP components have revealed Trf4 (36% identical) and Air2 homologs present in *N. crassa* forming evidence for a TRAMP-like complex (Altschul et al., 1997). FRH is not only proposed to be a component of TRAMP,

but is a vital member of the circadian oscillation within *N. crassa* where it was first identified as a binding partner of the frequency (FRQ) protein homodimer (Cheng et al., 2005). These two pathways share FRH as a common factor, however the pathways may or may not be functionally linked **(**Figure 1-4). *N. crassa* has been well characterized to understand circadian oscillation pathways making FRH an ideal candidate for the continued study of an Mtr4-like protein.

FRH AIDS IN REGULATION OF CIRCADIAN OSCILLATION

In *N. crassa*, FRH not only functions as an RNA helicase but also as an essential component for circadian oscillation (Cheng et al., 2005) (Figure 1-5). FRH participates in a negative feedback loop of the oscillation pathway through interactions with transcription factors White Collar 1 and 2 (WC-1 and WC-2) and Frequency (FRQ) (Shi et al., 2010). The positive arm of the circadian clock is regulated by the White collar proteins forming a heterodimeric White Collar Complex (WCC) (Shi et al., 2010). Historically, much of what is known about circadian oscillation pathways can be traced back to studies conducted using *N. crassa* as a model system (Aronson et al., 1994).

In *N. crassa*, the circadian oscillation begins with the WCC binding to the *frq* promoter to transcribe *frq* mRNA in the nucleus (Froehlich et al., 2003), which is then assumedly transported to the cytosol and translated into FRQ protein. Immediately following translation, the intrinsically disordered FRQ binds to FRH and together they form the FRQ/ FRH Complex (FFC) (Hurley et al., 2013). The FFC is then transported to the nucleus where it can associate with casein kinase 1 (CK1) (Hurley et al., 2013). FRQ is then phosphorylated on the C-terminus and in regions where FRQ interacts with FRH, promoting stability (Heintzen and Liu, 2007). The WCC is then inhibited by the FFC

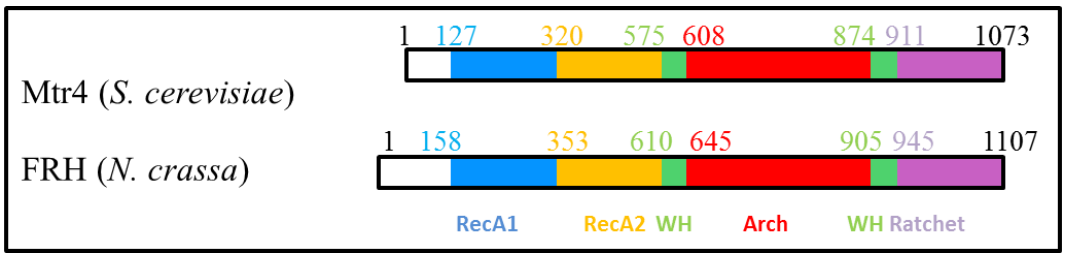

Figure 1-3. Domain alignments of scMtr4 and FRH. scMtr4 (top) is 1073 amino acids long while FRH (bottom) is 1107 amino acids in length. The core domains are all present in FRH based on alignment with the scMtr4 sequence with RecA1(blue), RecA2 (yellow), Winged helix (green), Arch (red), and Ratchet helix (purple). The two N-termini (white) are different in length and do not align well. Residue numbers are indicated for the beging and end of the sequences as well as the start of each domain.

through phosphorylation that breaks up the WCC and *frq* interaction (Liu and Bell-Pedersen, 2006).

Consequently, the WCC leaves the nucleus and *frq* levels decrease (Froehlich et al., 2003). Meanwhile, the phosphorylation of FRQ continues on the N-terminus until the Skp/Cullin/F-box containing (SCF) complex recognizes the hyper-phosphorylated FRQ and ubiquitinates FRQ (Guo et al., 2010; Hurley et al., 2013). The ubiquitinated FRQ is then degraded by the proteasome (Heintzen and Liu, 2007). The degradation of FRQ triggers the release of WC-1 from the FFC allowing the cycle to begin again (Dunlap and Loros, 2004). In total, the cycle takes about 22.5 hours to be completed (Aronson et al., 1994).

Furthermore, the WCC and FRH inhibition requires that FRQ be bound to FRH, since both proteins contribute to the binding surface for the WCC (Guo et al., 2010). Also, the phosphorylation level of FRQ is an indication for the circadian oscillation period (Hurley et al., 2015). All FRQ proteins are bound to FRH within the cell and FRQ does not need to be dimeric for this association (Cheng et al., 2005; Guo et al., 2010).

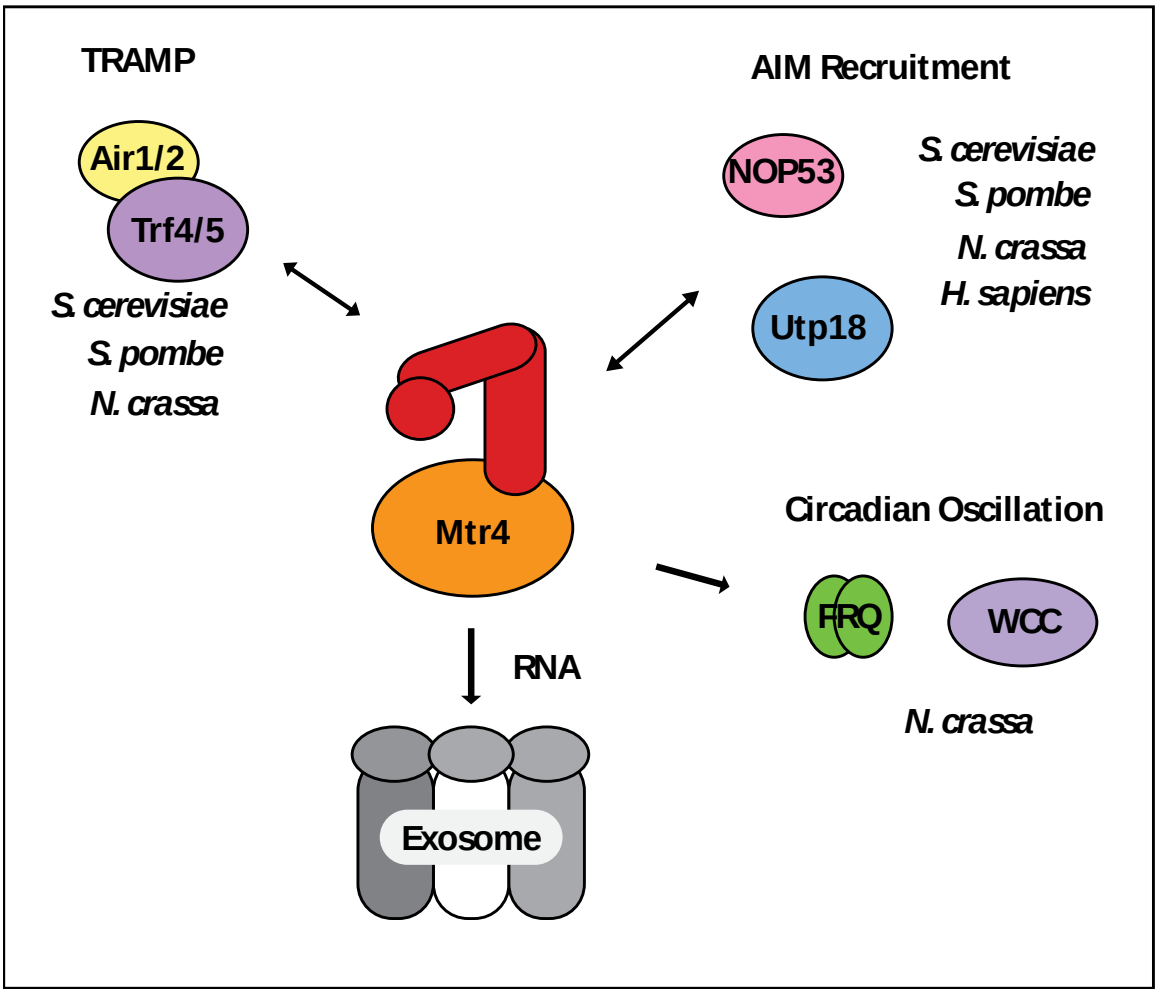

Figure 1-4. Mtr4 Complexes. Mtr4 is in the middle providing RNA to the nuclear exosome. Some of the known complexes formed by Mtr4 homologues are shown by double headed arrows if they are known to be involved in RNA surveillance. TRAMP (Trf4/Air2/Mtr4pPolyadenylation complex) and homologues have been identified in *S. cerevisiae*, *S. pombe*, and *N. crassa* (Johnson and Jackson, 2013). AIM motif recruitment factors and homologues have been identified in *S. cerevisiae*, *S. pombe*, *H. sapiens*, and *N. crassa* (Thom et al., 2015). Circadian oscillation complexes of Mtr4 homologue FRH have been identified in *N. crassa* with the FRQ and WCC (Cheng et al., 2005). These complexes are represented with a regular arrow because the complexes have not been shown to directly interact with the exosome.

Interestingly, the ratio of FRQ to FRH within the FFC complex has been observed to be 2:2 or larger over size exclusion chromatography (Lauinger et al., 2014). With FRH

stabilizing FRQ, FRQ can interact with the WCC and inhibit transcription activation of the *frq* gene promoter (Figure 1-5A) turning off the positive feedback loop of circadian oscillation (Liu et al., 2003). The FFC is formed by an interaction between FRQ residues 774-782 (Guo et al., 2010) and FRH residues 100-150 on the disordered N-terminus of FRH (Hurley et al., 2013). Conversely, when FRH is missing or the FRH-FRQ interaction is disrupted, FRQ is hypo-phosphorylated, and rapidly degraded (Guo et al., 2010). This is accompanied by lower levels of WC1 and WC2 indicating that the positive feedback loop is also disrupted by the loss of FRH (Guo et al., 2010). These findings indicate that the negative and positive feedback loops rely on one another for balance throughout circadian oscillation.

Conversely, the positive arm of the feedback loop occurs when WCC is not inhibited by the FFC. During positive regulation the WCC binds to the *frq* promoter and recruits the chromatin remodeling complex SWI/SNF (Hurley et al., 2015). The SWI/SNF complex, along with other proteins, removes a nucleosome from the DNA and brings the transcription start site into proximity of the *frq* gene for transcription (Hurley et al., 2015). This *frq* mRNA is then either translated into protein or degraded by FRH to either continue or halt the cycle (Guo et al., 2010). Interestingly, throughout the oscillation period levels of FRQ fluctuate while FRH levels remain constant (Cheng et al., 2005).

FRH is essential to this pathway by providing a chaperone to guide the intrinsically denatured FRQ homodimer (Hurley et al., 2013). Yet, FRH can also transverse from the cytosol to the nucleus while the majority of FRQ resides within the nucleus (Cheng et al., 2005; Hurley et al., 2013). Although, helicase activity seems unnecessary for FRH to participate in the circadian oscillation pathway, FRH performs this essential role to

maintain rhythmicity (Hurley et al., 2013). The separation of these activities was determined through a series of point mutations to residues specified for helicase function in FRH homolog scMtr4 (K208E, E294Q, S326L, and R580P) (Hurley et al., 2013). Specifically, the K208E mutation was designed to cripple nucleotide binding, E294Q to eliminate ATP hydrolysis, S326L to block unwinding activity, and R580P to stop both ATPase and nucleotide binding (Hurley et al., 2013). In each case, rhythmicity was observed in *N. crassa* strains containing each FRH mutant (Hurley et al., 2013). Even if helicase activity is not essential for FRH to participate in circadian oscillation, the link FRH forms between the circadian oscillation and RNA surveillance pathways may be important for maintaining expression levels and cellular availability of some RNAs.

FRH IS AN ESSENTIAL RNA HELICASE

FRH is a unique and essential RNA helicase necessary for growth and the negative feedback-loop of daily circadian oscillations (Guo et al., 2010). *Neurospora* cell extract analysis has enabled the estimation that ~40% of FRH is bound to FRQ at all times leaving ~60% free FRH within the cell (Cheng et al., 2005). In order to determine the necessity of FRH, a quinic acid (QA)-controlled FRH knockdown RNA hairpin was inserted into a wild type *Neurospora* strain (Guo et al., 2010). The addition of QA allowed for the controlled reduction of FRH by ~90% and resulted in arrhythmic strains (Guo et al., 2010). Levels of *frq* mRNA were also lowered coinciding with lower levels of FRQ protein (Cheng et al., 2005). This decrease in FRH was accompanied by a buildup of cellular *frq* mRNA which is also a substrate for FRH (Guo et al., 2010).

The accumulation of *frq* mRNA when FRH is knocked down is an indication that FRH is essential to the lifecycle of certain mRNAs (Cheng et al., 2005). Furthermore, evidence

that FRH associates with the catalytic exosome cofactor Rrp4 strengthens the argument that FRH is involved in exosome-mediated RNA processing (Figure 1-5B) (Guo et al., 2009). A recent article demonstrated how diverse RNA substrates travel to the exosome machinery through proteins that recruit scMtr4 to these RNAs. These yeast recruitment factors Nop53 (a homolog of the human tumor suppressor PICT1) and Utp18 part of the 90S pre-ribosome both contain an arch interaction motif (AIM) to recognize and bind the scMtr4 arch domain (Thom et al., 2015). This AIM motif is found on the N-terminal domain and is conserved across various species including the Nop53 and Utp18 *N. crassa* homologs (Thom et al., 2015). Due to this conservation the *N. crassa* Nop53 and Utp18 homologs are predicted to similarly recruit the exosome machinery using the arch domain of FRH, as seen in yeast (Thom et al., 2015). This unique interaction capable of recruiting the exosome machinery to specific RNA substrates demonstrates a critical role of the arch. Another feature of the AIM interacting region found in scMtr4 is the conserved arginine R678 (Jackson et al., 2010) in the arch or KOW region of the scMtr4. This region is recognized by the AIM sequence and the residue is conserved in the FRH arch corresponding to residue R712 (Thom et al., 2015). Since the arch domain is unique to Mtr4-like helicases (Jackson et al., 2010) this could point to a similar role in different species. Even though the FRH arch maintains secondary structure similarity with Mtr4, the primary sequence differs between species with only a 39% identity and 62% similarity between primary sequences for the arch region (determined using BLAST (Altschul et al., 1997)). These differences may be due to the role of FRH in circadian oscillation and will be further discussed in the summary and conclusions chapter.

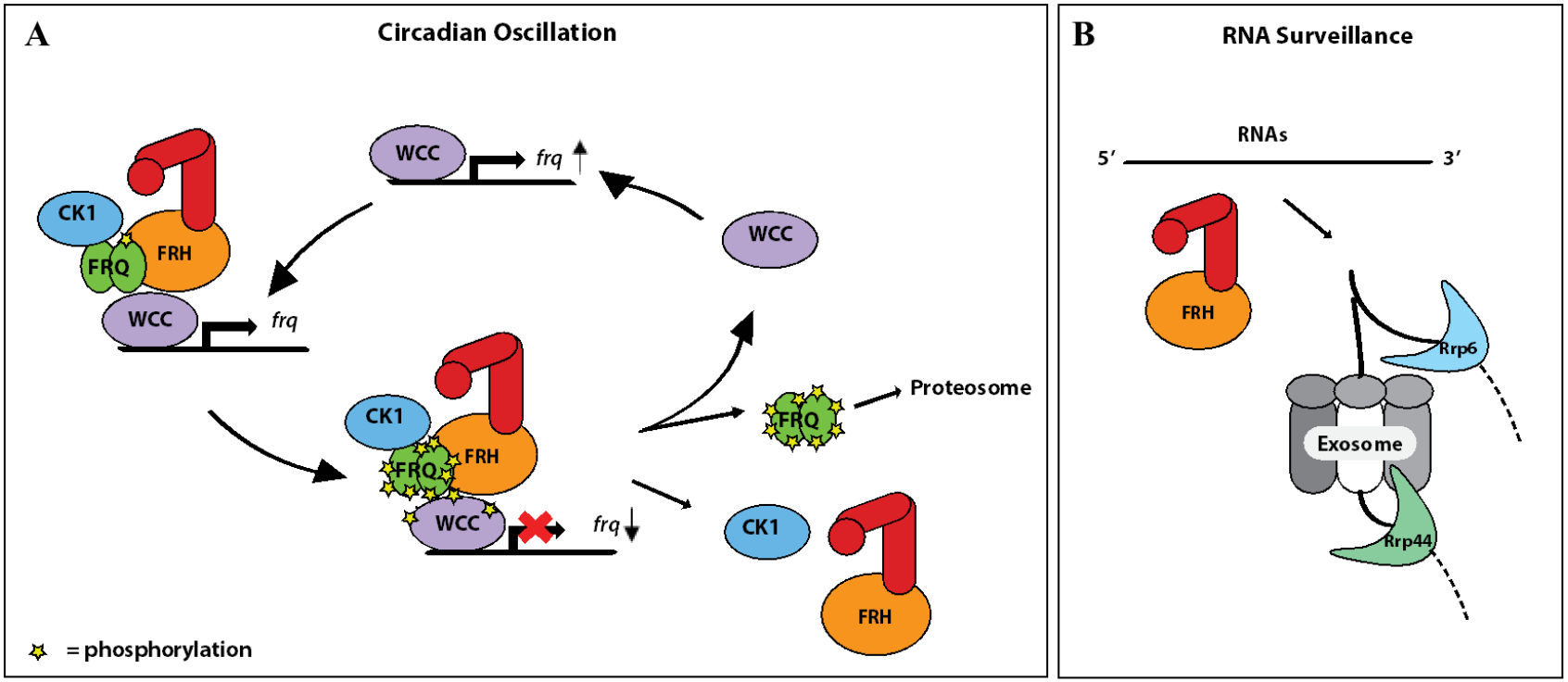

Figure 1-5. Roles of FRH. Circadian Oscillation. A - The WCC promotes the transcription of the *frq* promoter increasing the levels of FRQ protein. FRQ forms a complex with FRH and CK1 to inhibit the transcriptional regulation of the WCC through phosphorylation. FRQ is periodically phosphorylated throughout the day and eventually degraded by the proteasome. This release of the FFC and WCC interaction allows the WCC to start the cycle anew (Hurley et al., 2013). **RNA Surveillance. B –** FRH is proposed to participate in RNA surveillance through interactions with the exosome and associated proteins (Guo et al., 2009).

CONCLUDING REMARKS

Maintaining levels of RNA in the cell is critical to cellular stability and the prevention of diseases. Understanding the cellular machinery involved in maintaining these RNA levels through exosome-mediated RNA surveillance is still an incomplete picture. Much of the knowledge gap lies within how RNA substrates interact with Mtr4-like helicases before they are processed by the exosome. Model helicases such as FRH are essential to this process and need to be studied to understand the macromolecular interactions involved. FRH is a unique example of an Mtr4-like helicase due to its participation in the circadian oscillation pathway (Cheng et al., 2005). Although it is assumed that FRH and scMtr4 are highly similar this seems to ignore the unique role FRH provides *N. crassa* through the circadian oscillation pathway. With FRH being the only known link between circadian oscillation and RNA surveillance in *N. crassa* (Guo et al., 2009), intrinsic differences in scMtr4 and FRH may be present. Biochemical and structural characterization of FRH, the essential Mtr4-homolog found in *N. crassa*, is presented in this work. Insights into how FRH interacts with RNA through activity assays and structural analyses are provided. Implications of this work include further understanding of a unique RNA helicase and consequently expansion of RNA surveillance knowledge. This unique opportunity to study an RNA helicase that links two separate cellular pathways may yield some surprising results.

CHAPTER 2

COMPREHENSIVE COLLECTION OF METHODS USED TO CHARACTERIZE FRH

INTRODUCTION

The frequency-interacting RNA helicase (FRH) protein from *N. crassa* is of particular interest because of its dual role as part of the circadian oscillation pathway and as an Mtr4-like helicase in RNA surveillance, thereby linking these two important regulatory pathways. Aside from connecting these pathways, little is known about FRH structurally and functionally. It has been proposed that FRH functions similarly to scMtr4, in RNA surveillance based on sequence alignments and secondary structure predictions. However, while the FRH protein has been shown to play an important role in circadian oscillations, the yeast Mtr4 has no such identified function. This difference highlights a unique role for FRH not previously observed in other Mtr4-like helicases. With this knowledge FRH was identified as a unique Mtr4-like helicase to study for this dual role and to further the understanding of RNA surveillance. In this chapter, outlined are the methods utilized to express, purify, crystallize, and biochemically analyze FRH.

The coding sequence for FRH was first received in a pET_Duet vector containing both FRH and FRQ from the Yi Liu lab (University of Texas Southwestern, Dallas). The vector is named SJJ 175 and stored in the Johnson lab plasmid archive. This is where I

began work on the project. FRH contained an N-terminal, six Histidine tag and was cloned into a TOPO expression vector using restriction sites KpnI and EcoRI, to be separated from FRQ. Initial expression of recombinant FRH in *E.coli* BL21 DE3 codon plus cells yielded poor solubility in various growth conditions and was thus unsuccessful. These conditions included ZY, LB, and Super broth media, along with different expression times ranging from 5-30 hours and temperatures for growth at 16° C, 22° C, and 37° C. FRH was then transferred to an expression vector containing an N-terminal TEV cleavable GST affinity tag to improve solubility (SJJ 192). This strategy was adopted from Lauinger *et al*. supplemental information where soluble expression of FRH was observed (Lauinger et al., 2014). A second FRH construct was also made by truncating the first 128 amino acids from the N-terminus to aid in crystallization trials (SJJ 193). Once solubility was achieved, a purification protocol was developed. In short, the purification entails the use of Glutathione S-transferase affinity resin (Gold Bio), a Hi-Trap Heparin column (GE Healthcare), and size exclusion chromatography (SEC). The developed protocol is described in detail in the PROTEIN PURIFICATION section. Once FRH protein was purified to >95%, we began crystallization trials.

FRH was first crystallized at 8.8 mg/ml (1:1 drop ratio) in Hampton Research Index screen conditions containing 0.2 M Sodium Malonate or 0.2 M Sodium Citrate both at pH 7.0 with 20% 3350 PEG solution. These conditions were further optimized by altering the pH, precipitant percentage, and concentration of FRH. Also, utilized was a micro-seeding approach to create preformed nucleation sites for the crystals. The optimization of and final conditions used to crystallize FRH are described below in CRYSTALLIZATION OF

FRH CONSTRUCTS. Crystals of FRH yielded two full data sets one of the Full Length FRH at 3.5 Å and another of the N-terminally truncated Δ128 FRH at 3.25 Å. Both of these datasets yielded structures that were solved using molecular replacement to obtain phasing data and refinement of the data was performed using PHENIX software. Full data collection and specifications are described within this chapter.

Also observed within the symmetry mates of these structures was a structural dimer of FRH. Analysis of the dimer with surface area interface calculator PISA (Proteins, Interfaces, Structures, and Assemblies) revealed that the interaction is predicted to be biological, with a perfect complex interface significance score (Krissinel and Henrick, 2007). The structure was further analyzed through the use of another interface classifier called EPPIC (Evolutionary Protein-Protein Interface Classifier) where the FRH dimer was ranked to be biological (Duarte et al., 2012). The presence of the dimer was also explored in various conditions using crosslinking analyses combined with size exclusion chromatography. FRH was further characterized as a helicase in unwinding assays with a poly-A RNA substrate. Published activity assays for scMtr4 helicase activity have provided values for which to use as a benchmark comparison for FRH. Within this chapter are the comprehensive methods used to study FRH. The information provided should allow for the continued study of FRH.

METHODS

Construct Design

Full length or the first 128 amino acids N-terminally truncated (Δ128) FRH DNA sequence from *Neurospora crassa* were inserted into a GST-pDB PSI *E. coli* expression vector coding for a TEV cleavable, N-terminal, GST tag (Figure 2-1). The Δ128 construct was designed to be similar to the scMtr4 Δ74 construct by removing amino acids predicted to be unstructured on the N-terminus through secondary structure prediction software (Jones, 1999). Removing the GST tag through TEV cleavage leaves two extra N-terminal residues on the FRH sequence.

Protein Expression

FRH protein was recombinantly expressed in an *E. coli* BL21 (DE3) codon+RIL cell line. Protein expression was induced using an auto-induction protocol and ZY media. Traditional IPTG expression with LB media did not produce soluble protein. Cultures were grown under Kanamycin and Chloramphenicol (25 mg antibiotic to 500 ml media) antibiotics at 37º C for 5 hours and room temperature for 28 hours to achieve optimum protein expression. Cells were harvested at 10,000 rpm for 30 minutes and stored at -80º C.

FRH Protein Purification

Cells were lysed manually through the use of lysozyme and sonication. GST-affinity, heparin affinity, and size exclusion techniques were used to purify FRH to

approximately 95% purity. TEV cleavage of the GST tag was performed through dialysis after the heparin affinity step for approximately 6-8 hours at 4° C. Lysis and wash buffers contained 20 mM NaH_2PO_4 (pH 7.5), 2 mM beta-mercapto ethanol, 5% glycerol, and 50 mM salt. First, the cell pellet (30 g) was re-suspended on ice in five times the volume of cell mass in Lysis buffer supplemented with 1X Lysozyme, Pepstatin, Leupeptin, and PMSF (GoldBio). Cells were broken by sonication at 60% power duty cycle 6 for 6 rounds of thirty seconds sonicating and thirty seconds resting. Followed by clarification at 18,000 rpm for 25 minutes at 4° C. The soluble fraction was then allowed to batch bind to lysis buffer equilibrated GST resin for 2 hours at 4° C. The flow through was then collected and the resin washed with 50 ml of Lysis buffer. GST elution buffer containing 50 mM Hepes (pH 8.0), 10 mM reduced L-Glutathione, 2 mM beta-mercapto ethanol, and 50 mM salt was used in elutions. Three 10 ml elutions were performed with a 10-minute incubation period between each. All elutions were then loaded onto a Heparin affinity column. Heparin affinity buffers included 50 mM Hepes (pH 7.5), 5% glycerol, 2 mM beta-mercapto ethanol, and 50 mM or 1 M salt. The column was washed with 25 ml of the 50 mM salt buffer before fractionation. Fractions of 2.5 ml volume were collected once the salt gradient of 8 column volumes began. Before the final purification step, FRH fractions were pooled for TEV cleavage. TEV cleavage was performed in dialysis membrane in 500 ml of TEV buffer containing 50 mM Hepes, 100 mM NaCl, 5% glycerol, and 10 mM beta-mercapto ethanol. After one hour of dialysis, a second sample of TEV was added and the dialysis buffer exchanged then dialysis was allowed to proceed for 6-8 hours more. Upon completion of dialysis and TEV cleavage the FRH solution was concentrated to 5 ml in a

50 kDa concentrator at 20,000 rpm and 4° C for intervals of 12 minutes. Concentrated FRH was then loaded onto a 320 ml Superdex column for final purification. SEC buffer contained 50 mM Hepes (pH 7.5), 2mM beta-mercapto ethanol, 5% glycerol, and 100 mM salt. All purification buffers were filtered with a 0.22 μm nitrocellulose filter and kept at 4° C. Purification steps were monitored using SDS PAGE gel electrophoresis (Figure 2-2) and Unicorn UV chromatograms.

Tips for FRH preps

- After cell lysis all possible steps need to be performed in the 4° C cold room this ensures little degradation throughout the purification.
- For the lysis of cell pellets larger than 10 grams or greater than 1 L of ZY growth, batch binding should be performed in a 250 ml bottle and remain on a shaker at 4° C throughout the full 2 hours.
- For eluting off of GST resin the sample should be agitated and allowed to incubate for 10 minutes at 4° C between elutions. All elutions will be loaded onto the Heparin column.
- For the Heparin elution FRH is unaffected at how long the gradient is, for good separation of contaminants the salt gradient can range from 6-10 CV. Anything longer is unnecessary for FRH. When the chromatogram is visible pool all peak fractions for TEV cleavage and dialysis. This is important to do quickly because the dialysis needs 6-8 hours. Less than 6 hours can cause only partial cleavage, the

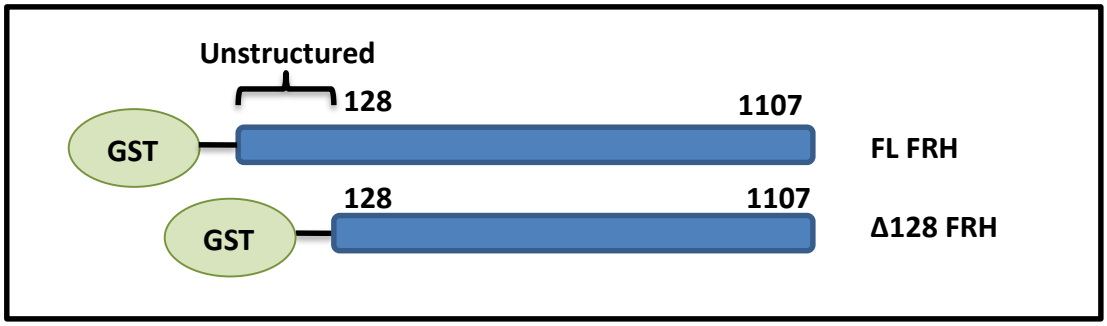

Figure 2-1. Expression Constructs. FRH is recombinantly expressed in a pDB-GST PSI vector. The resulting protein contains a glutathione S-transferase tag (green) linked by a TEV cleavage (black) site to the full-length or 128 truncated FRH protein (blue). The N-termini to the 128 residue is denoted as unstructured from structural prediction analyses.

Superdex gel above (Figure 2-2 Gel D) is an example of only a 5-hour cleavage from before this was known. It is pertinent to do the full cleavage because separation is difficult otherwise and the GST-FRH only appears as a small shoulder on the AKTA chromatogram.

- During concentration of FRH before sizing the TEV within solution may crash out at speeds of 1800 rpm. This does not affect the FRH, if precipitation of TEV occurs filter the sample with a 0.22-micron syringe filter.

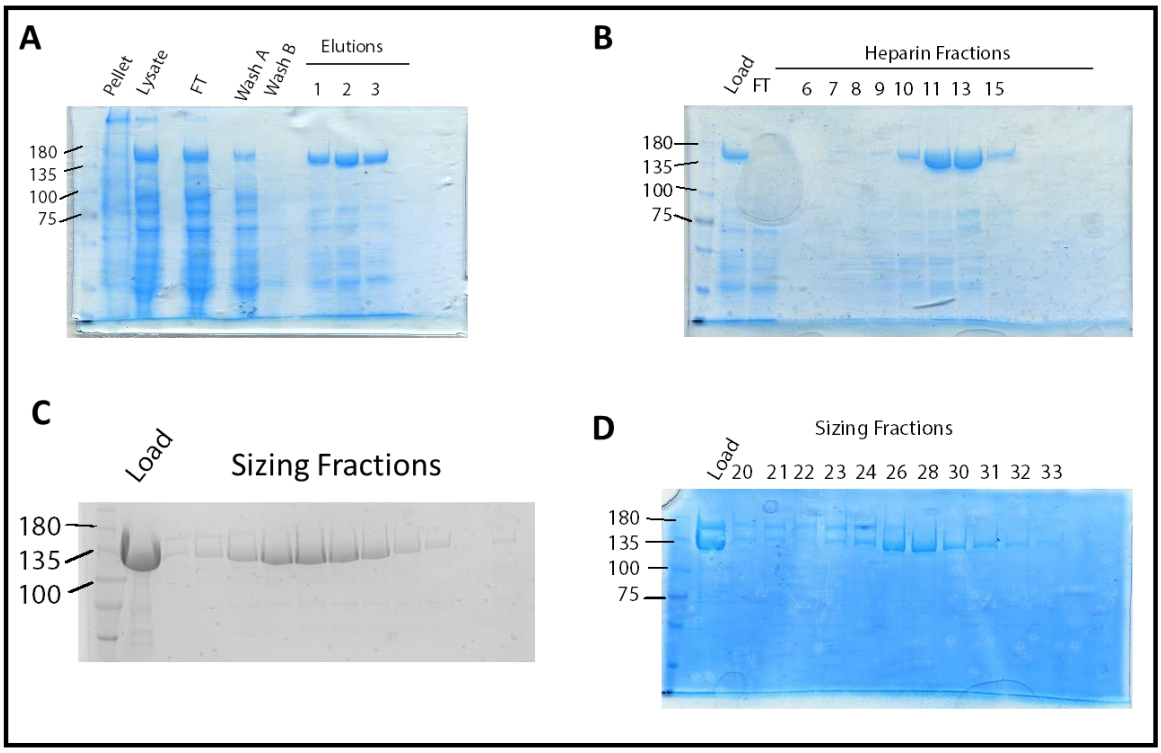

Figure 2-2. Protein Purification. SDS gels of the purification steps are shown above. **Gel A-** GST affinity resin step including lanes for the cell pellet, lysate, flow through (FT), wash A, wash B, and three 10 ml Glutathione elutions. **Gel B-** 5 ml Hi-Trap Heparin affinity column showing what was loaded onto the column (load), the FT of the column, and samples of fractions from a salt elution gradient. **Gel C**- FRH after a complete TEV cleavage step run over a 320 ml Superdex column. **Gel D**- An example of an incomplete TEV cleavage step followed by a 320 ml Superdex run. Both the GST-FL FRH (156k Da) and the FL FRH (124 kDa) are clearly visible on the gel.

Activity Assays

Unwinding activity was determined using a helicase assay developed by Wang et al 2008. This assay monitors displaced P^{32} labeled 16 nt ssRNA from dsRNA utilizing a 5' five amino acid overhang of either Poly-Adenine nucleotides or random nucleotides (Figure 2-3B). Within the reaction tube 40 mM MOPS pH 6.5, 100 mM NaCl, 0.5 mM

$MgCl_2$, 5% glycerol, 0.01% NP-40 substitute, 2 mM DTT, 1 U/µl Ribolock (Thermo Fisher), and protein were combined for a total volume of 120 µl. ~0.2 nM P^{32} labeled RNA substrate was added and reactions initiated with 1.6 mM ATP/$MgCl_2$. The reaction was incubated at 30° C in a controlled water bath. Time points were collected at 0, 1, 2, 5, 10, 20, and 60 minutes while being quenched with an equal volume of 2X stop reaction buffer containing 1% SDS, 5 mM EDTA, 20% glycerol, 0.1% bromophenol blue and 0.1% xylene cyanol. Samples were then run on a 15% Native TBE polyacrylamide gel for 110 minutes at 100 volts. Next the gel was wrapped in saran wrap and exposed through use of a phosphor screen for 24 hours and then imaged with a STORM phosphor imager utilizing Image Quant to analyze the image (Amersham Biosciences). Time points were plotted in Kaleidagraph based on the fraction of unwound RNA over time and the initial rates plotted on a Michaelis-Menten plot to determine the K_{unwind} rate (min^{-1}) and the $K_{1/2}$ concentration of FRH. Unwinding activity was performed in triplicate with three separate FRH purifications utilized for verification example phosphor image of gel shown in Figure 2-3A below.

Crystallization of FRH Constructs

Optimization from the original Hampton Index conditions of 0.2 M Sodium Malonate or 0.2 M Sodium Citrate both at pH 7.0 with 20% 3350 poly ethylene glycol (PEG) solution began by altering the PEG and pH. Two sitting drop hand trays were designed to test these (Hampton research), one at pH 6.5-8.0 for 0.2 M Sodium Malonate the other tray for 0.2 M Sodium Citrate at pH 5.5- pH 7.0 in 0.5 steps both trays ranged

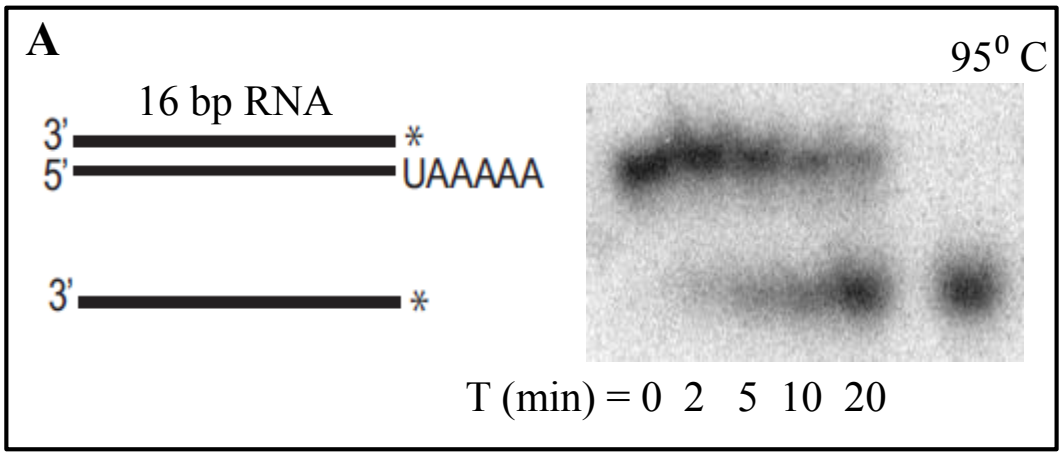

B R16 (top strand) = 3'CGCAGAAAUGCCACGA 5'
R22A (poly-A overhang) = 5'GCGUCUUUACGGUGCUUAAAAA3'

Figure 2-3. Helicase Activity of FRH. A - Helicase substrate of dsRNA and ssRNA product depicted next to location on the phosphor screen exposure of a helicase gel collected by a STORM scanner. Reaction time points and 95^0 C boiled control are labeled on phosphor image **B-** Sequence of RNA substrate (R22A) used in helicase assays. Substrate contains a 5 poly-A tail as a 3' overhang.

from PEG 14%- 24% in 2% increments. From these trays crystals only grew at room temperature in the Sodium Citrate conditions containing 24% PEG 3350 at pH 5.5 or 6.0. The crystals were small at this point but, the pH 6.0 were just large enough to loop and test with the Johnson lab home source. These crystals diffracted between 7-8 Å resolution with a distinct pattern indicative of a protein crystal (Figure 2-4A-B). At this stage many of the crystals grew on the plastic pedestal within the sitting drop tray and were broken when trying to loop so hanging drop trays were utilized to prevent this. Optimization continued with the 0.2 M Sodium Citrate pH 6.0 conditions because it yielded diffracting protein crystals. 3350 PEG values were narrowed to 18-22% in a 1:1 protein: well drop ratio to

produce crystals that diffracted between 4-5 Å at the Johnson lab home source (Figure 2-4C-D). Crystals were also grown using microseeding dilutions and using a 2:2:1 protein: well: seed ratio these crystals. The microseeded crystals in the 100,000 and 1,000,000 seed range produced crystals that diffracted around 4 Å at SSRL. The two data sets collected utilized microseeds of 1,000,000 for the 3.5 Å for the FL FRH crystal and 1,000,000 for the 3.25 Å Δ128 FRH crystal. Crystallization was shown to occur between 3 to 7 mg/ml final concentration of FRH in the drop however, higher and lower values were not tested.

Data Collection, Structure Determination, and Model Refinement

Crystallographic data were collected from 30 to 3.5 Å for the full length FRH construct and 30 to 3.25 Å for the Δ128 FRH construct at the Stanford Synchrotron Radiation Laboratory (SSRL) on beamline 7-1. Data were processed using HKL2000 (Otwinowski and Minor, 1997). The FRH crystals belong to space group $P3_121$ with cell dimensions and angles listed in the table below. Both crystals contain one molecule in the asymmetric unit supported by Matthews coefficient =2.6 $Å^3$/Dalton; 52.69% solvent (Kantardjieff and Rupp, 2003; Weichenberger and Rupp, 2014). Initial phases were defined using molecular replacement from homolog scMtr4 (PDB ID 4U4C) for the first FRH structure and for the second structure the 3.5 Å FRH structure was utilized. Refinement with the PHENIX software included using rigid body and grouping B factor settings while restricting TLS parameters to maintain visible secondary structure. Optimization of XYZ coordinates and stereochemistry or sidechains was used to account for the positioning of sidechains and reduce the clash score of the molecule. Further used, was the ability to reset

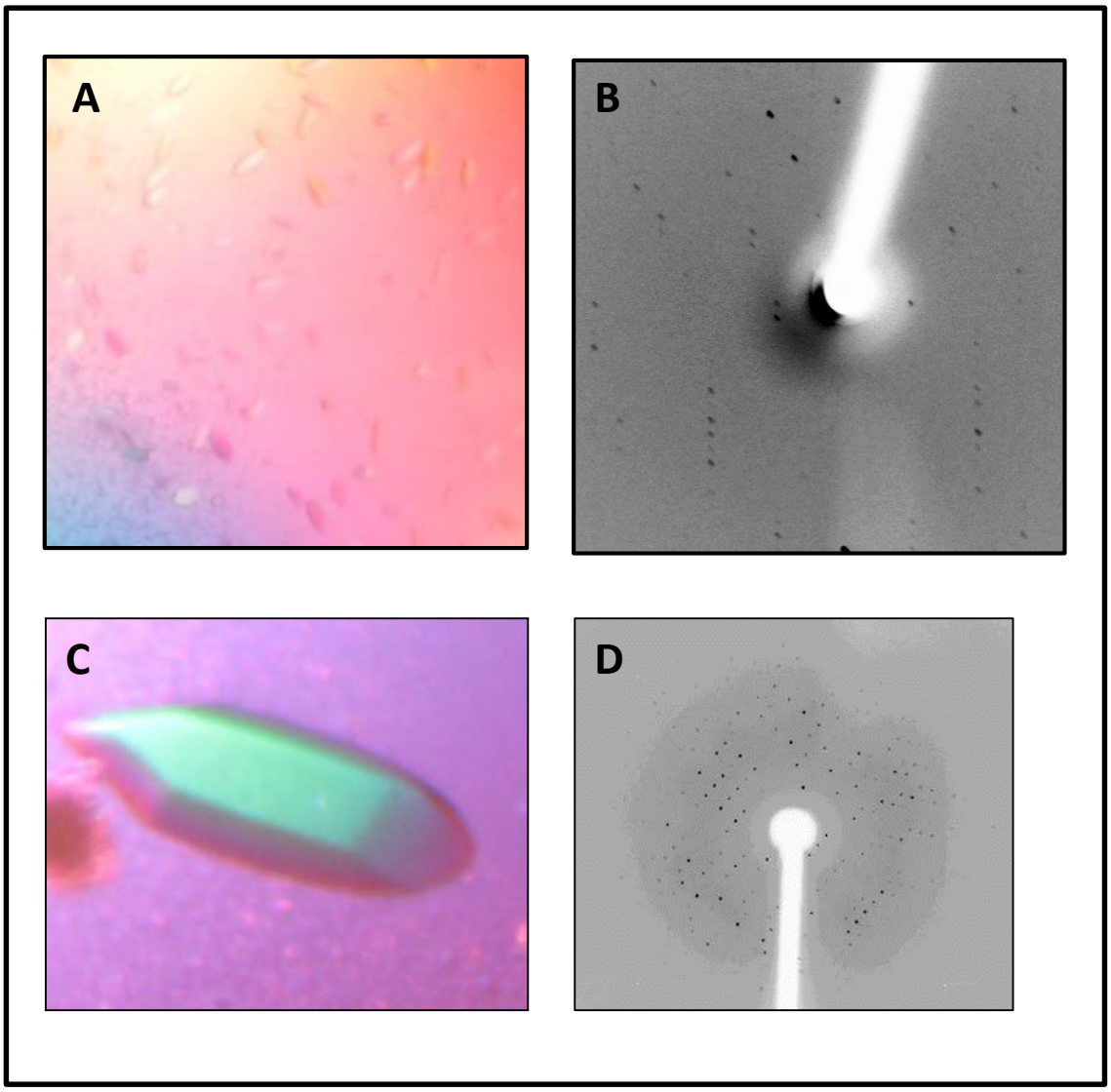

Figure 2-4. FRH Crystallization and Diffraction. A- FRH crystals from the first round of optimization in 0.2 M Sodium Citrate pH 6.0 and 24% 3350 PEG. **B-** First diffraction pattern resulting from crystal in 8A of FRH at 7-8 Å resolution. **C**- Depicts an optimized FRH crystal in 0.2 M Sodium Citrate pH 6.0, 20% 3350 PEG, containing a 1,000,000 diluted micro-seed sent to SSRL **D**- Diffraction pattern resulting from crystal at SSRL

B factors for the sidechains before each refinement to maintain a lower final B factor after refinement. Final refinement statistics are displayed for each crystal in Table 2-1 below.

Crosslinking

Assay was performed in (sizing buffer) 50 mM Hepes (pH 7.5), 100 mM salt, 5% glycerol, 2 mM beta-mercapto ethanol, and 0.01% Triton-X 100. 0.01-0.05% Glutaraldehyde crosslinking reagent was added to 0.2-1.0 µM FRH. Crosslinking was performed at 30^0 C for 5-15 minutes with the reaction quenched with 10 µl 1M Tris pH 8 and a 1:4 ratio of 4X SDS sample dye and boiled for 5 minutes before SDS-PAGE analysis (Figure 2-5).

Size Exclusion Chromatography

1 mg/ml FRH samples were prepared using FRH sizing buffer in 100 µL volume with or without 10 µL of 2.3% glutaraldehyde (high percentage to ensure crosslinking). Control and crosslinked samples were incubated at 37° C for 15 minutes and quenched with 20 µL of 1 M Tris pH 8.0. Samples were then desalted using an equilibrated 0.5 ml Zeba spin column (Thermo Fischer). Desalting was performed at 4° C and 8,000 rpm. Samples were then filtered using a 0.22 µM spin filter (Thermo Scientific) at 8,000 rpm for 30 seconds. 10 µl samples of purified FL FRH or crosslinked FRH were loaded onto an equilibrated 3 ml Superdex 200 Increase 5/150 GL (GE Healthcare) and run at 0.15

ml/min. Samples were analyzed using Unicorn 5.11 chromatogram software and SDS gel electrophoresis.

Table 2-1. Data Collection and Refinement. 3.5 Å FL FRH and 3.25 Å Δ128 FRH crystal data sets after refinement

Data Collection and Refinement		
Beamline	SSRL 7-1	SSRL 7-1
Space group	$P3_121$	$P3_121$
Cell dimensions		
a, b, c (Å)	118.5, 118.5, 179.6	118.9, 118.9, 181.6
α, β, γ (°)	90.0, 90.0, 120.0	90.0, 90.0, 120.0
Resolution (Å)	30 – 3.51 (3.64 - 3.51)	30 – 3.25 (3.39 - 3.25)
No. of reflections		
unique	18761	24009
total	352123	513013
I/σ(I)	22.7 (1.0)	74.8 (1.1)
Completeness (%)	99.9 (100)	100 (99.8)
Redundancy	21.2 (21.3)	21.0 (20.8)
$CC^{1}/_{2}$	0.99 (0.308)	1.0 (0.305)
R_{work}/R_{free}	0.2478/0.2998	0.3014/0.3345
Total no. protein atoms	7198	7202
B factors (Å^2)	164.6	120.6
RMSD bonds (Å)	0.011	0.007
RMSD angles (°)	1.75	1.497
Ramachandran Favored (%)	88.6	88.8
Ramachandran Outliers (%)	4.7	4.6

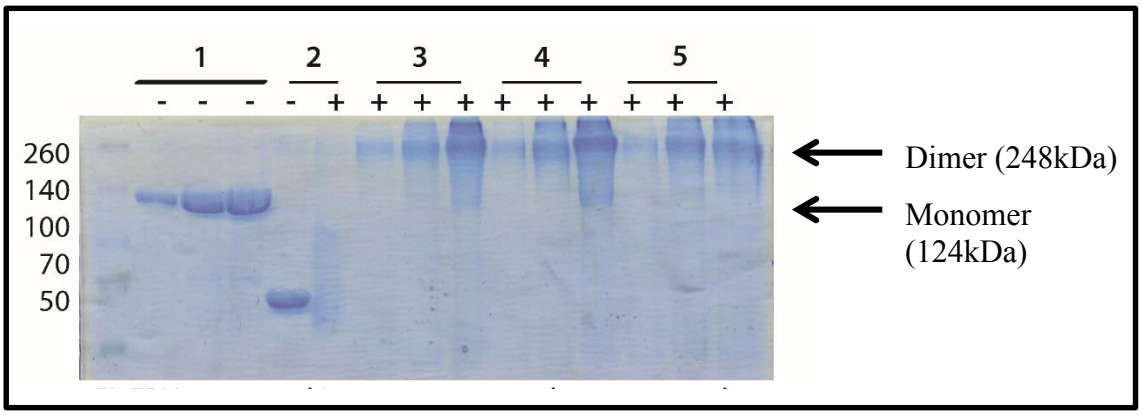

Figure 2-5. Glutaraldehyde Crosslinking of FRH. Group 1 lanes are FRH (1.6 µM, 4 µM, 8 µM) without Glutaraldehyde. Group 2 are a BSA without and with reagent. Groups 3, 4, 5 are FRH in 0.2 M NA Citrate pH 6, 50 mM Hepes pH 7.5, and a 50/50 mixture of both buffers respectively. FRH was kept at the same concentrations as the negative controls. 2.3% Glutaraldehyde was added and allowed to react for 5 minutes before quenching.

Dimer Interface Validation

Both Proteins, Interfaces, Structures, and Assemblies (PISA) (Krissinel and Henrick, 2007) and interface prediction software Evolutionary Protein-Protein Interface Classifier (EPPIC) (Duarte et al., 2012) independently determined the surface area between dimers to be 2444.9 Å^2 per monomer. The interaction includes 14 hydrogen bonds and 4 salt bridges. Structural validation for the interaction being biologically relevant is the perfect 1.0 Complex Formation Significance Score (PISA) (Krissinel and Henrick, 2007).

CONCLUDING REMARKS

The comprehensive methods presented in Chapter 2 are for FRH expression, purification, crystallization, and activity assays. The structural analyses performed are repeatable for any crystallographic data set. With the presented methods as a basis, future

FRH work should be repeatable. Within Chapter 3, ANALYSIS OF FRH STRUCTURAL AND BIOCHEMICAL RESULTS, the results from the methods in Chapter 2 are discussed.

CHAPTER 3

ANALYSIS OF FRH STRUCTURAL AND BIOCHEMICAL RESULTS

INTRODUCTION

FRH is an essential RNA helicase, necessary for the circadian oscillation and RNA surveillance pathways within *N. crassa* (Guo et al., 2009). FRH has been extensively studied for its chaperone role in the circadian oscillation pathway of *N. crassa,* which does not seem to be dependent upon helicase activity (Hurley et al., 2013). However, FRH has been demonstrated to be an essential helicase necessary for cell viability through a possible role in RNA surveillance (Cheng et al., 2005) . This dual functionality in two essential pathways has not been observed for other known RNA helicases, making the link FRH forms between the circadian oscillation pathway and RNA surveillance in *N. crassa* intriguing. Due to this unique role and the need to further understand exosome-mediated RNA surveillance, FRH was pursued. Structural and biochemical characterization are presented in this work to start to answer how FRH functions as a unique Ski2-like RNA helicase.

RESULTS

FRH Purification and Expression

In brief, a purification strategy was developed for FRH. First, FRH was recombinantly expressed in *E. coli* through utilizing a GST expression vector. Following cell lysis, FRH was extracted through the use of GST and Heparin affinity resins. A TEV cleavage was then used to remove the GST tag and size exclusion chromatography

performed as a final purification step. FRH was then concentrated and stored in a 25% glycerol containing buffer at -80° C until use. These methods are discussed in detail in the Chapter 2.

FRH Structural Analysis

Structurally, FRH has been predicted to be highly similar to scMtr4. This has been the speculation due to sequence identity (53%) and similarity (73%) from NCBI BLAST (Altschul et al., 1997). Even though these two proteins are predicted to be similar, no structural information has been determined for FRH to elucidate the actual structure. In this work, the solved crystal structure of FRH is presented. The structure is accompanied by an explanation of how phasing was addressed, electron density fitted, and how the data was refined.

FRH was first collected at 3.5 Å resolution with a $P3_121$ space group using the SSRL beamline 7-1. Crystallization was performed with the hanging drop vapor diffusion method. Conditions included; 11.1 mg/ml FRH, 0.2 M Sodium Citrate pH 6.0, 20% 3350 Poly-Ethylene Glycol (PEG), and a 1: 1,000,000 crystal seed from a previous hand tray in a 1:1:1 ratio. Molecular replacement was used with a scMtr4 structure (Falk et al., 2014) (PDB ID: 4U4C) to define the phasing for the dataset. Interestingly, the arch domain of FRH had a different conformation than the available scMtr4 structures. This conformational difference meant the entire FRH arch domain had to be built using secondary structure elements visible within the density. One of the major challenges of working with this resolution was determining where the fist portion of the arch was. One helix within the FRH fist domain was clearly visible within the electron density map

allowing for a fist to be modeled in. A unique morphology of a Ski2-like helicase became visible as each portion of the arch domain was modeled in (Figure 3-1). Not only were the arch domain and fist regions in a drastically different conformation than previously observed in scMtr4 structures but, a structural dimer within the crystal was also present. All other Mtr4-like and Ski2-like helicases have been observed to be monomeric thus far, making the FRH dimer interesting. Another crystal structure of FRH, excluding the first 128 residues was later solved to 3.25 Å and displayed the same dimeric structure. These findings have elicited deliberations on this dimer for biological relevance which will follow within this chapter in the section titled FRH DIMER. Structural analyses of domain movement and comparison to other Ski2-like helicases will follow.

FRH Maintains Ski2 Core Domains

FRH is a Ski2-like helicase maintaining the two RecA domains within the helicase core RecA1 (blue) and RecA2 (yellow), a winged helix (green), and the ratchet helix (magenta) (Figure 3-1) (Johnson and Jackson, 2013). The FRH core (colored) was aligned to the winged helix domain of the available scMtr4 structures (grey) for comparison of the core domains (Figure 3-2). RMS values, generated in PyMol (Table 3-1), indicate that the FRH core domains adopt a conformation most similar to the "TRAMP-like" scMtr4 structure (Falk et al., 2014) (PDB ID: 4U4C). This similarity to a partial complex of scMtr4, may be due to the cores in the dimeric FRH packing together. However, domain motion may be shifted in comparison because they are from different organisms. From these alignments, one can conclude that the overall core domains seen in Ski2-like helicases are still observed with the FRH core. Even though the core domains remain

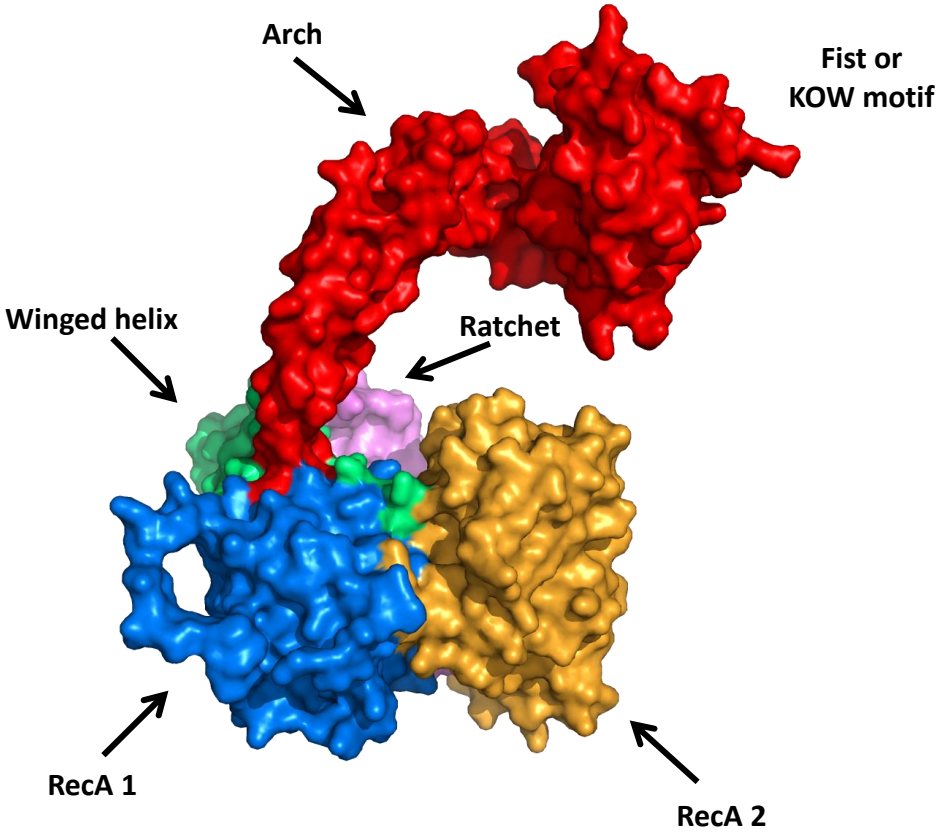

Figure 3-1. Crystal Structure of FRH. Surface representation of the FRH crystal structure generated using PyMol. Domains colored blue for RecA 1, yellow for RecA 2, green for the winged helix, red for the arch, and magenta for the Ratchet helix domain. The KOW or fist region of the arch is also labeled.

similar, differences in the arch domain are visible. The arch domain is a unique characteristic of Ski2-like helicases being inserted into the winged helix domain (Jackson et al., 2010). The arch protrudes from the middle of the winged helix (domain 3) out of the helicase core creating a domain 3a (Johnson and Jackson, 2013). The known scMtr4 arch domains are compared structurally to the FRH arch domain in the section titled ARCH DOMAIN. Similarity in the core domains of FRH and scMtr4 suggest a similarity in

activity that will be discussed in the CHARACTERIZATION OF HELICASE ACTIVITY section. However, the noticeable difference in the arch domains will be discussed first.

Arch Domain

The arch domain is an accessory domain inserted within the core winged helix domain 3 in Ski2-like helicases (Jackson et al., 2010). The arch domain contains two helical arms ascending and descending from the globular fist region that is positioned above the helical core. The arch appears to be somewhat flexible with the focal point of movement spanning from the winged helix and the connection between the helical arms and fist (Johnson and Jackson, 2013). A comparison of the conformation seen for the scMtr4 arch (Taylor et al., 2014)(PDB ID: 4QU4) and the FRH arch are shown below demonstrating a 12.1 Å shift in the helical arms to be further over the helical core and a 33.7 Å "flip of the wrist" to move the fist higher above the core, than previously observed with scMtr4 (Figure 3-3). These conformational changes display a different overall shape allowed within the arch domain of FRH. The difference in the FRH arch may be due to crystallographic packing and/or differences in protein interactions. Furthermore, this difference in conformation could indicate a role for the arch domain in FRH not present for scMtr4. In fact, the interaction between the WCC and FRH arch domain is necessary for the circadian oscillation pathway (Shi et al., 2010). The responsible residue for this interaction has been identified as a conserved arginine within the arch domain (R806) (Shi et al., 2010). This demonstrated role for the arch in *N. crassa* agrees with an arch recognition mechanism to recruit Mtr4-like helicases. A similar recruitment model has been identified for Mtr4 with AIM recruitment factors Nop53 and Utp18

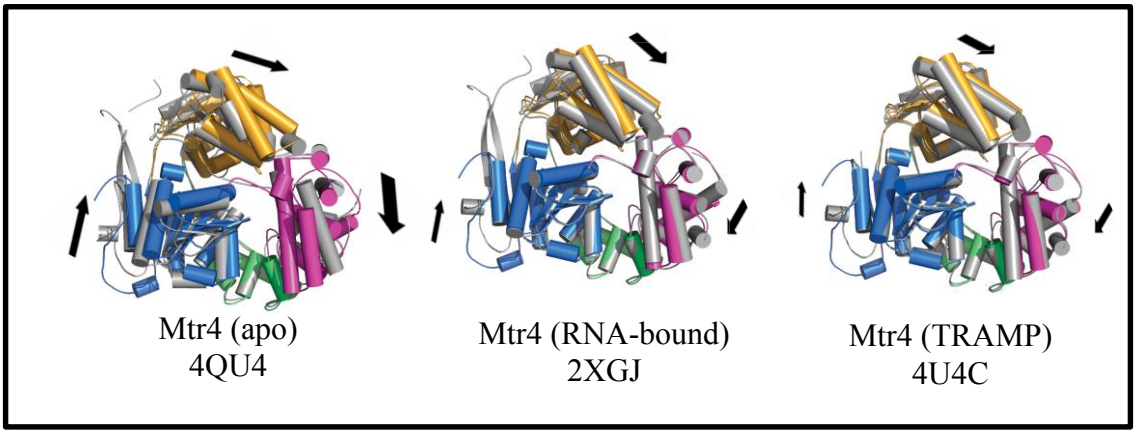

Figure 3-2. Winged Helix Alignments. Core alignments using the winged helix between the FRH core (colored) and three scMtr4 structures. scMtr4 structures include 4QU4 no substrate bound (apo), 2XGJ containing a 5 nucleotide poly-adenine substrate, and 4U4C containing peptides of TRAMP components.

Table 3-1. RMS values (PyMol) of FRH compared to Mtr4 core domains. RMS measured in Å, when the winged helix domain is aligned as shown in Figure 3-2.

Domain	***4QU4***	***2XGJ***	***4U4C***
RecA1	3.217	1.088	0.880
RecA2	3.322	2.663	1.824
Ratchet Helix	5.002	1.557	1.388

(Thom et al., 2015). Despite these findings, the overall role and function of the arch in RNA surveillance is still under investigation. Currently, the FRH arch has had little characterization however, studies with the scMtr4 arch have begun to answer this question.

Previously, the scMtr4 fist has been shown to bind structured hypo-modified tRNA however, not to bind single stranded poly-A RNA (Johnson and Jackson, 2013). The binding of structured RNA indicates that structured RNA substrates can interact with the arch. Due to their structural similarity and the conservation of the KOW motif, (structured RNA binding motif) it is predicted that FRH also uses the fist region to bind structured RNAs. This binding may be used as a guide for the RNA into the helicase core however, further investigation is needed to determine this. The fist has also been demonstrated to promote RNA substrate unwinding in scMtr4 (Taylor et al., 2014). This finding supports a model where the arch is guiding the RNA into the core domains of the helicase. The fist has also been shown to act as a recognition site for chaperone proteins to recruit Mtr4 to the exosome machinery for the processing of specific RNA substrates (Thom et al., 2015). Due to structural similarities and the conservation of key residues, these roles are likely to transverse to the *N. crassa* system as well.

Characterization of Helicase Activity

In order to characterize FRH helicase activity, assays were performed as for scMtr4 (Jackson et al., 2010; Taylor et al., 2014; Wang et al., 2008). Previously, domain 4 residues in the scMtr4 ratchet helix have been shown to be involved in unwinding rates of RNA substrates (Taylor et al., 2014). The authors pointed out the conservation of residues along the ratchet helix across species and determined residue R1030 (corresponding to FRH

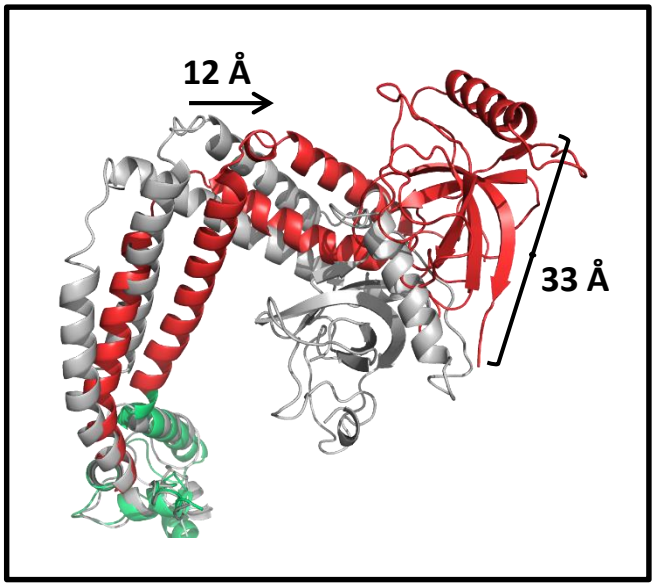

Figure 3-3. Arch Alignment. FRH arch (red) and winged helix (green) aligned to the corresponding scMtr4 (PyMol) (PDB ID: 4QU4) region (grey). This alignment demonstrates the conformational differences observed between the crystal structures.

residue R1063) to control the preference for a poly-A RNA substrate (Taylor et al., 2014). This observation may indicate that FRH prefers the same type of poly-A RNA substrates. To begin to answer this question, FRH activity has been characterized with the same RNA substrate containing a poly-A tail used for scMtr4. The RNA unwinding results are shown in Figure 3-4. The FRH K_{unwind} max is 0.562 +/- (0.094) min^{-1} and the $K_{1/2}$ 766.06 +/- 252.79 nM. These results are still initial values with an R^2 of only 0.976 and a large error bar at the 1200 nM FRH concentration. Further assays will need to be conducted to address these disparities. The reported values for scMtr4 K_{unwind} max is 0.59 +/- 0.05 min^{-1} and the $K_{1/2}$ 252 +/- 60 nM (Taylor et al., 2014). While the K_{unwind} max of FRH and scMtr4 are fairly similar there is a large discrepancy of the $K_{1/2}$ values. The difference in the $K_{1/2}$ may be attributed to the large error bar at 1200 nM. The similarity of the rates is probably due

to the conservation between their catalytic regions (Johnson and Jackson, 2013). Based on the similarity of the K_{unwind} max values, FRH is a comparable helicase to scMtr4. Although characterization of helicase activity is an important comparative measure, the helicase assay is not designed to observe how the RNA substrate is recognized by the helicase.

The processes of how RNA substrates are recognized by FRH and scMtr4 are still not fully understood. As discussed previously, other proteins such as Nop53, Utp18, (Thom et al., 2015) and the TRAMP complex can recruit scMtr4 to RNA substrates for exosome-mediated degradation (Vanacova et al., 2005). The ability of the arch domain to bind structured RNAs has implicated the arch to participate in substrate recognition (Taylor et al., 2014). Further preference of these RNAs to be poly-adenylated is regulated by the ratchet helix however, this polyadenylation is not necessary for unwinding to occur (Taylor et al., 2014). This ambiguity in RNA substrates makes determination of an overall recognition model difficult. It is reasonable to speculate that processing of different RNA substrates are based on the presence of different recruitment proteins.

FRH Dimer

FRH stands out as a lone example of a dimeric Ski2-like RNA helicase. All other RNA helicases within this family are represented as monomers (Fairman-Williams et al., 2010). Dimeric RNA helicases are not prevalent in the literature with only several examples available. One example is, MjDEAD a DEAD-box helicase from *Methanococcus jannaschii* that forms an N-terminal dimeric association through beta sheet secondary structure (Story et al., 2001). Another DEAD-box helicase HERA from *Thermus thermophiles* forms a C-terminal dimer (Rudolph and Klostermeier, 2009).

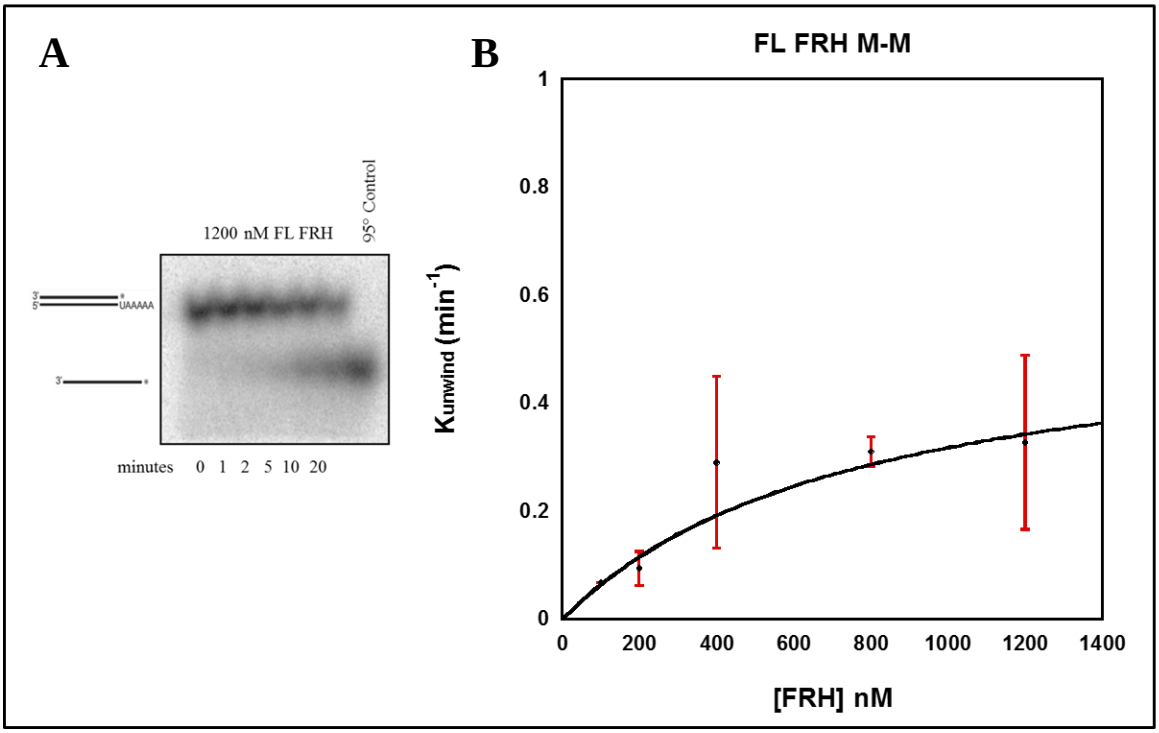

Figure 3-4. Helicase Assay. A- Helicase substrate of dsRNA and ssRNA product depicted next to location on the phosphor screen exposure of a helicase gel collected by a STORM scanner. Reaction time points and 95^0 C boiled control are labeled on phosphor image. **B-** Initial Michaelis-Menten cure from FL FRH with R22A substrate depicted above with error bars from triplicate data collection.

MDA5 forms a C-terminal dimer (Berke and Modis, 2012) and UAP56/URH49 together from an N-terminal dimer through alpha helical secondary structure all from *Homo sapiens* (Zhao et al., 2004). Despite these examples, only the MjDEAD protein forms a dimer through a beta sheet extension similarly to FRH however, none have a dimer interface highly similar to the FRH dimer. This lack of a similar dimeric interface makes comparison and validation of the dimer FRH difficult. Specifically, the FRH dimer is located on the N-terminus through a beta sheet secondary structure continuation and amino acid interactions spanning from the core to the arch domain (Figure 3-5). When comparing the

N-terminal region of dimeric FRH to the monomeric scMtr4, it is apparent that scMtr4 has a secondary structure difference preventing the association seen in FRH. The scMtr4 N-terminus forms a long beta sheet hairpin (β hairpin) connected to the RecA1 core domain, while FRH has a disordered N-terminus. The function of this β hairpin structure is currently unknown aside from preventing the same dimer interface seen in the FRH crystal structure. PISA analysis has indicated the dimer is formed through 14 hydrogen bonds and four salt bridges formed from sidechain residues (Table 3-2). The dimer interface (Figure 3-5) forms a surface area of 2444.9 Å^2 per subunit (Krissinel and Henrick, 2007). When analyses under surface interface validation software (Duarte et al., 2012; Krissinel and Henrick, 2007) (PISA & EPPIC) the FRH dimer is ranked as likely to be biological. From PISA, the dimer has a perfect complex significance score of 1 and EPPIC ranked the interaction to be biologically relevant. Results from EPPIC classifier are listed in Table 3-3. Both of these analyses predict that the dimer is biological and not an artifact of the crystallographic conditions.

PISA and EPPIC utilize unique algorithms to assess the validity of an observed dimer interface. PISA has an 80-90% success rate in identifying biological complexes (Krissinel and Henrick, 2007) and EPPIC has a success rate of 88% as tested against a PDB-wide search (Baskaran et al., 2014). PISA utilizes a surface area approach to eliminate interactions that do not contain enough interaction area between proteins and also predicts bonds between interfaces (Krissinel and Henrick, 2007). EPPIC utilizes a different approach relying on evolutionary data from proven biological interfaces to predict sequence entropy within homologous protein sequences (Duarte et al., 2012). The EPPIC classifier also utilizes a geometric analysis to compare the ratio of core and rim residues

present in a crystal structure (Duarte et al., 2012). Core residues are broken into two classes 95% or greater buried residues are used for core geometry prediction and 70% or greater are used for evolutionary prediction and rim residues are the remainder (Duarte et al., 2012). The agreement between the PISA and EPPIC analyses provides strong structural support for the validity of the observed FRH dimer.

Despite the structural evidence suggesting an FRH dimer, biochemical support for this conclusion is lacking. Previous studies have shown FLAG tagged FRH is unable to pulldown V5 tagged FRH (Hurley et al., 2013). However, multimeric states are observed by gel filtration when FRH is in complex with FRQ (Lauinger et al., 2014). Further validating the significance of the observable crystallographic dimer was pursued through crosslinking assays combined with size exclusion chromatography. Glutaraldehyde chemical crosslinking was utilized in various conditions where dimeric molecular weight was observed. The dimeric molecular weight was observed in concentration of 50 mM and 100 mM NaCl (Figure 3-6). The 50mM concentration was utilized to demonstrate conditions that are most likely below the NaCl concentration in the cell while the 100 mM concentration was utilized to demonstrate a higher concentration. Crosslinked and untreated FRH samples were also ran on a size exclusion column to determine size elution profiles. The goal of this experiment was to determine if untreated FRH ran at the dimeric FRH size by comparing treated and untreated FRH samples. However, the effectiveness of the crosslinking reagent made isolation of a dimeric FRH difficult to obtain, due to the formation of other multimeric species. This result may indicate multimeric species are also favored in solution. Although the dimer formation results were inconclusive, further

optimization of crosslinking conditions to isolate a pure dimeric FRH sample can be pursued to utilize this technique in the future. Determining the biological significance of the observed FRH dimer structure may be necessary to determine roles performed by FRH.

Despite the convincing structural argument for the FRH dimer, other Ski2-like helicases have been observed to be monomeric. In fact, the well characterized scMtr4 has always been observed to be monomeric. In an effort to determine any significant differences that would allow formation of a dimer in FRH but not scMtr4, the topology of the two N-termini were compared (Figure 3-7). Amino acid sequence alignments of the N-terminus along with secondary structure indicate one more β-sheet present on the N-terminus of scMtr4 that is not present in FRH or the RecA1 domain (Figure 3-7A). The first β-sheet observed in FRH corresponds to the second in scMtr4 and is much shorter containing only five residues in comparison to thirteen residues. The first two β-sheets in scMtr4 have been previously identified as an N-terminal β-hairpin (Weir et al., 2010). This β-hairpin folds across both RecA1 and RecA2 domains on the scMtr4 core providing stability and appears to be unique to scMtr4 (Weir et al., 2010). In the absence of the N-terminal β-hairpin, FRH appears to provide stability by packing a second FRH molecule through the extension of the β-sheets in the RecA1 domains of both cores (Figure 3-7B).

CONCLUSION

Within this chapter the FRH structure and activity have been analyzed and compared to scMtr4. FRH is shown to maintain the core domains present in Ski2-like helicases with small domain motion of the core noted. The arch domain was aligned and

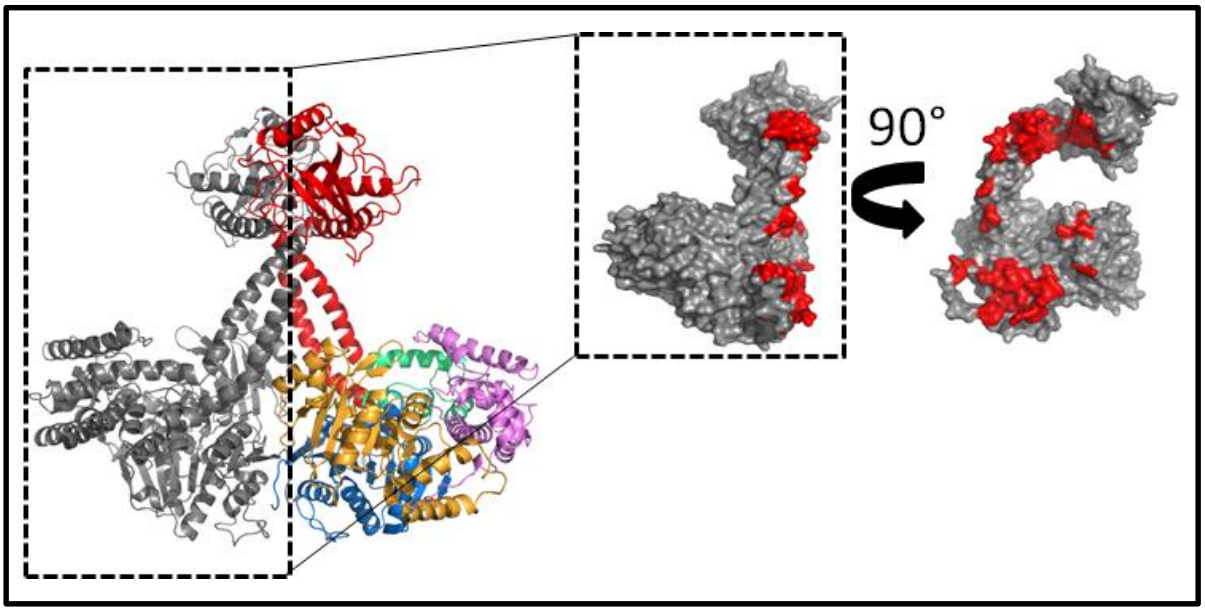

Figure 3-5. FRH Dimer Interface. FRH dimer displayed with two-fold symmetry seen in the crystal structure. Also displayed is the monomer in surface representation with the interface residues (red) and non-interface residues (grey).

compared to the scMtr4 arch demonstrating a different conformation observed in FRH. Helicase assays with the poly-A R22A substrate indicate that FRH has comparable activity to scMtr4. Also, the unique dimer observed in the crystal structure is still lacking biological significance and cannot be concluded from the work presented here. However, why scMtr4 cannot form this dimeric structure was investigated through the conflicting topology observed in the N-terminus. Future work to explore the FRH dimer and complete characterization of helicase activity are discussed in the Summary and Future Directives chapter to follow.

Table 3-2. PISA Interface Results.

Number of Residues		
Interface	72	7.8%
Surface	869	93.7%
Total	927	100.0%

Solvent Accessible Area (Å)		
Interface	2444.9	5.4%
Total	455520.4	100.0%

Hydrogen Bonding Residues		
Structure 1	**Structure 2**	**Distance (Å)**
LYS 168	VAL 142	2.77
GLN 150	ASN 146	3.12
HIS 149	ILE 147	2.79
ILE 147	HIS 149	2.99
LYS 376	ASP 156	2.98
ARG 657	GLU 381	3.06
ASN 883	ASN 883	3.63
VAL 142	LYS 168	2.77
ASN 146	GLN 150	3.12
ILE 147	HIS 149	2.79
ASP 156	LYS 376	2.98
GLU 381	ARG 657	3.06
ASN 883	ASN 883	3.63

Salt Bridge Residues		
Structure 1	**Structure 2**	**Distance (Å)**
LYS 376	ASP 156	2.98
ARG 657	GLU 381	3.06
ASP 156	LYS 376	2.98
GLU 381	ARG 657	3.06

Table 3-3. EPPIC Classifier Results of Evolutionary Core and Rim Residues. Core residues of evolutionary importance are utilized to identify residues likely to be conserved throughout homologues. Entropy is defined in EPPIC as the probability of an amino acid to be at a certain position in aligned sequences (Duarte et al., 2012).

Core Evolution Residues >70%

Residue	% Core	Entropy
SER 144	71	1.38
ASN 146	71	0.27
ILE 147	71	0.00
HIS 149	88	0.00
VAL 151	77	0.08
ALA 186	82	1.86
HIS 346	72	0.00
GLU 674	75	0.08
LEU 687	78	0.00
SER 718	97	2.16
SER 720	73	1.02
VAL 722	93	2.35
LEU 867	72	0.00
PRO 871	79	0.46
SER 875	81	0.81
PRO 876	94	0.58
VAL 879	99	1.45

EPPIC Totals and Scores

Total Core	Total Rim	Core-Rim Score	Core-Surface Score	Result
17 residues	56 residues	0.95	0.73	Biological

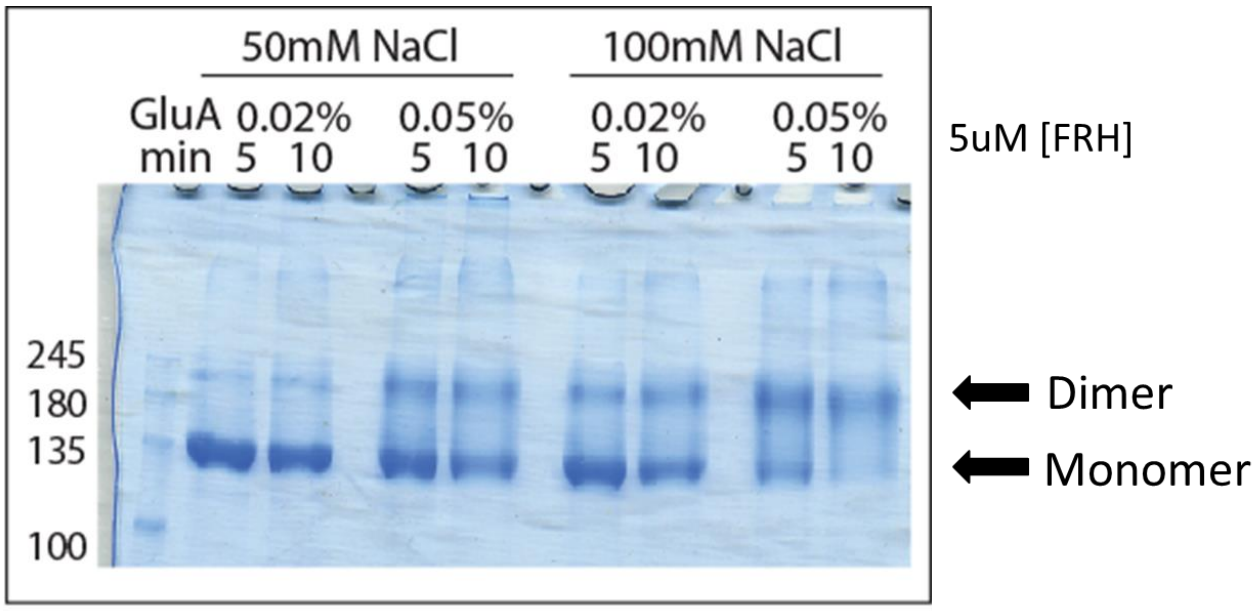

Figure 3-6. Optimization of Crosslinking Conditions for FRH. 5 µM FRH was crosslinked with either 0.02% or 0.05% glutaraldehyde at 30°C for 5 or 10 minutes with 50 mM of 100 mM NaCl. The utilization of two different salt concentrations indicates the crosslinking conditions show a salt dependent formation. The monomeric band (124kDa) and dimeric band (248kDa) are labeled on the gel.

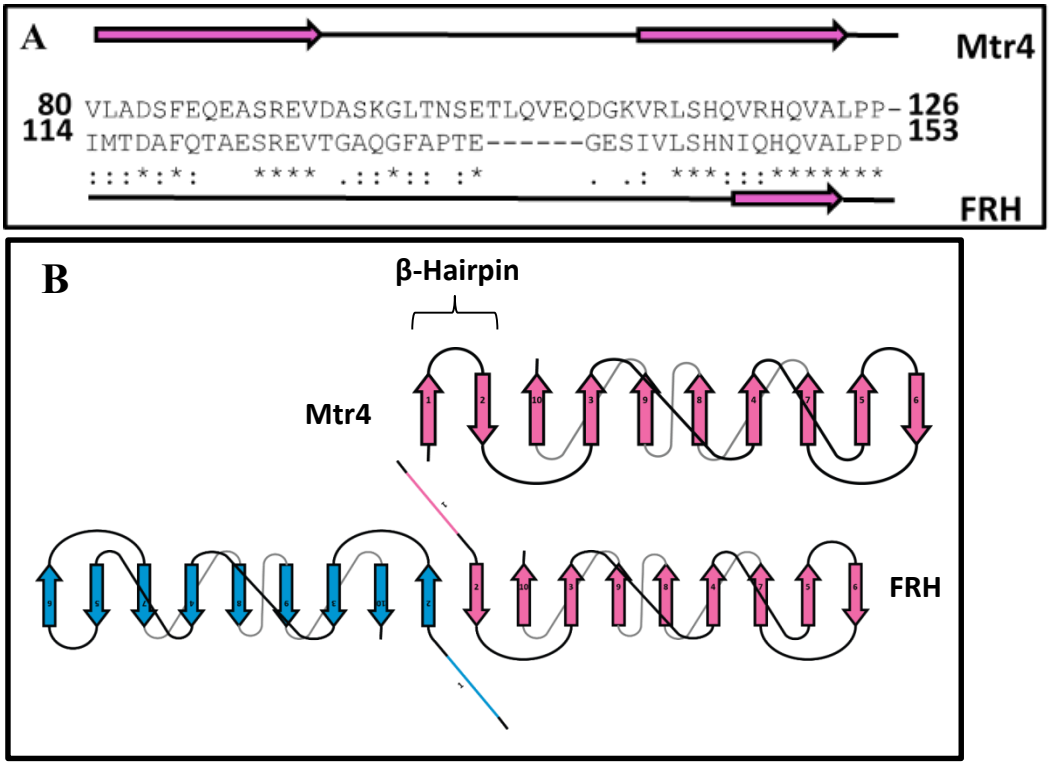

Figure 3-7. Comparison of the scMtr4 and FRH N-termini and Topology. A- Amino acid alignment of scMtr4 and FRH N-termini with β-sheet secondary structure indicated by arrows. **B**- Topology diagram of β-sheets seen in scMtr4 RecA1 domain monomer compared to two FRH RecA1 domains packing together in the dimer.

CHAPTER 4

SUMMARY AND FUTURE DIRECTIVES

FRH is a unique RNA helicase involved in two distinct cellular pathways. In this work a clear recombinant expression and purification protocol was outlined for studying FRH (Chapter 2). With these protocols, future studies can reliably replicate the presented work. Furthermore, crystallization conditions leading to the first structural information for FRH were presented at 3.5 Å with FL FRH and 3.25 Å resolution with Δ128 FRH (Chapter 2). The surprising structural dimer observed in the crystal structure still lacks conclusive biological evidence however, demonstrating dimeric formation through crosslinking, size exclusion chromatography, and structural analyses heavily point towards this conclusion (Chapter 3). The presented crystallization conditions can be followed to consistently crystallize FRH and further be used as a starting point for the crystallization of other FRH constructs. Characterization of helicase activity was performed with a poly-A RNA substrate previously used to characterize scMtr4. The initial results indicate that FRH is comparable to scMtr4 with this R22A substrate (Chapter 3). This work provides a starting point for future analyses proposed within this chapter.

BIOLOGICAL SIGNIFICANCE OF FRH DIMER

Elucidating the biological significance of the observed FRH dimer have proven difficult. Size exclusion chromatography has indicated multimeric FRH species are observed when FRQ is present (Lauinger et al., 2014). This technique was further used on a crosslinked sample of FRH in an attempt to compare the observed molecular weights of

untreated and crosslinked FRH. Although initial runs proved inconclusive, optimization of crosslinking condition should allow for the comparison of these samples in the future. A comparison of elution profiles would determine if untreated FRH runs as a monomer or dimer on a size exclusion column. Future constructs of FRH lacking the arch domain may also help elucidate more information on dimeric formation and significance. A crystal structure of an archless FRH construct could yield evidence for how the two cores are packing and if the arch is required to stabilize this interaction. An archless construct has been created and soluble expression verified for these studies. Explanation of the archless FRH design will follow.

ARCHLESS FRH DESIGN

The archless FRH vector was designed to be similar to the characterized archless scMtr4 construct. Removal of the arch was performed using a Gibson Assembly technique to remove the arch containing region and to insert residues from the DNA helicase Hel308 helicase (Figure 4-1A). Hel308 does not contain an arch domain. Instead, Hel308 contains a small loop (Buttner et al., 2007). This Hel308 loop region was previously used in the archless scMtr4 design to maintain core domain geometry and consequently, was used in the FRH archless design as well. Soluble expression of the GST tagged archless FRH protein (123kDa) is observed in both IPTG and auto-induction growth media (Figure 4-1B).

CONTINUED CHARACTERIZATION OF HELICASE ACTIVITY

For helicase activity, this work focused on the comparison of FRH to scMtr4 on a poly-A R22A substrate. The preference scMtr4 has for a poly-A substrate is accredited to

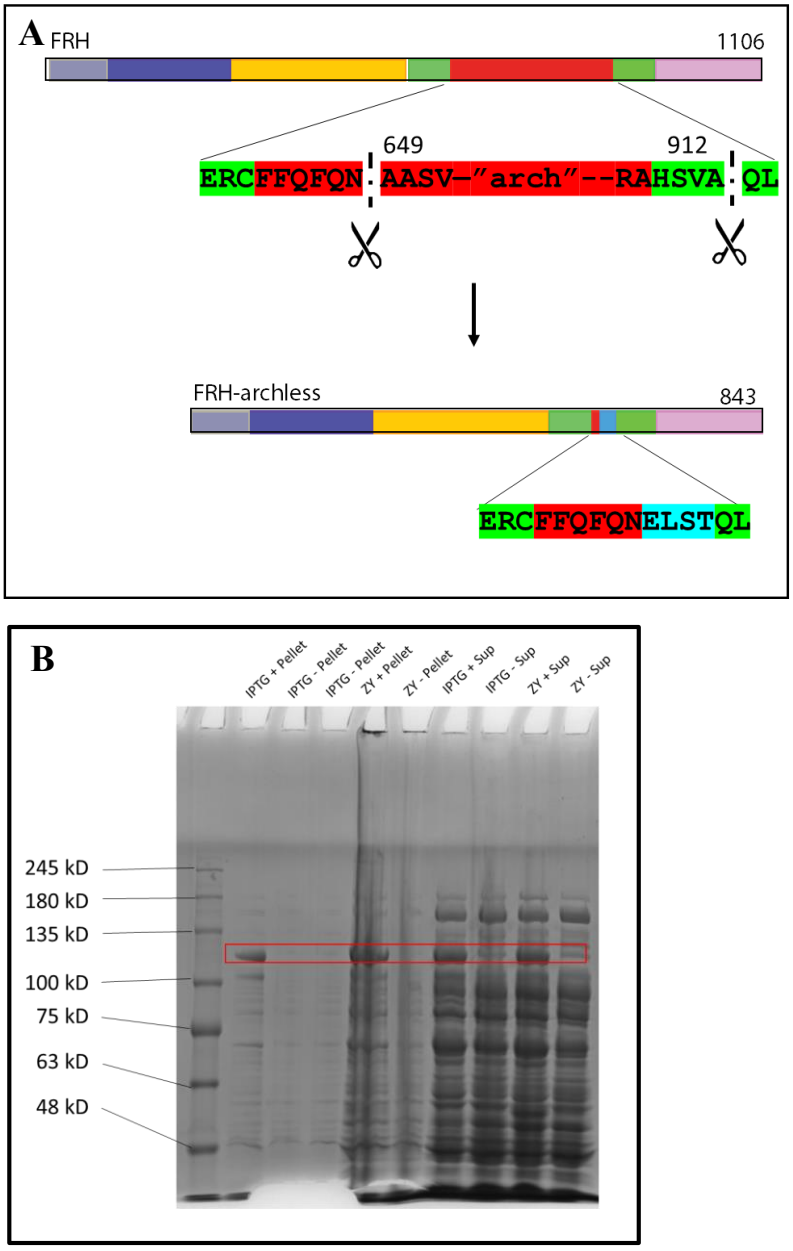

Figure 4-1. Archless FRH Design and Solubility. A- Schematic design for removal of the arch domain from FRH to create the archless FRH sequence with the insertion of the Hel308 loop (ELST). Sequences are color coded for N-terminus (grey), RecA1 (purple), RecA2 (yellow), winged helix (green), arch (red), Hel308 loop (light blue), and ratchet helix (pink). **B-** Soluble expression of GST tagged archless FRH (123kDa) seen in the IPTG + and ZY + supernatant samples.

the TRAMP complex found in *S. cerevisiae* (Taylor et al., 2014). TRAMP homologs have been identified in *N. crassa* yet, have not been studied. Since TRAMP in the *N. crassa* system has not been characterized, determining a preference for poly-A substrates on FRH would strengthen the model of FRH in a TRAMP complex and RNA surveillance. An archless FRH construct could be used in these helicase assays as well, to determine if differences exist between scMtr4 and FRH proteins. Studies with scMtr4 have indicated that an archless scMtr4 construct elicits a slow growth phenotype (Taylor et al., 2014). This archless scMtr4 was also observed to still unwind poly-A RNA substrates preferentially (Taylor et al., 2014). Performing helicase assays with the archless FRH could further the comparison between these two helicases.

CRYSTALLIZATION OF FRH CONSTRUCTS AND COMPLEXES

Structural characterization of FRH complexes has not been performed. Elucidating structural information about FRH complexes in both the circadian oscillation pathway and RNA surveillance pose to have significant impact in the understanding of both. Another question is of the biological significance of the observed FRH dimer, structures of FRH constructs and complexes could further elucidate the biological validity of this dimer. To start, an easily obtained structure should be of the archless FRH construct. An archless FRH structure could demonstrate if the arch domain is necessary for the dimer to form. The known FRH conditions can be used as a starting point to undergo crystallization trials of the archless FRH. If these conditions do not yield crystals broader conditions will be pursued.

Also, the current crystal structures of FRH are considered Apo structures without any substrates bound. Performing crystallization trials with RNA substrates and ATP

analogues could further be helpful in observing substrate interactions within the helicase core. Currently, the RNA-bound scMtr4 structure (2XGJ) provides information on interactions between RNA and the ratchet helix domain (Weir et al., 2010). Despite this, the RNA present is not long enough to visualize potential interactions between the other domains where another crystal structure may elucidate these interactions. Other structures of interest include complexes of FRH.

The FRQ protein minimal binding region to bind FRH has been identified in the literature (Guo et al., 2010). Exactly where this interaction occurs on FRH though has not been fully characterized but has been narrowed down to residues 100-150 on the N-termini (Hurley et al., 2013). Crystallization trials of FRH and the FRQ minimal binding region could determine the molecular nature of this interaction further and possibly shed light on the dimeric FRH observed in the crystal structure. Trials with an FRQ peptide can be performed in two ways. One strategy can attempt to soak the peptide into previously formed FRH crystals. Another approach can be to co-crystallize the peptide and FRH protein together. Both of these strategies have been attempted yielding no results however, preliminary results at this are not enough to say these strategies have been exhausted. Both strategies should be pursued to obtain a structure of the FRH-FRQ interaction. Many of the proposed crystallization trials have potential to impact the understanding of FRH in both the circadian oscillation and RNA surveillance pathways. FRH provides a model protein that has proved to be easy to work with and shown to repeatedly crystallize.

SUMMARY

This work has focused on the structural and biochemical understanding of the unique RNA helicase FRH. The crystal structure of FRH revealed a surprising dimer not

previously observed for other Ski2-like helicases. Although the structural analyses of the dimer are convincing, the biological significance of the dimer is still lacking conclusive results. In addition, a full purification protocol and initial activity assays are demonstrated for the future study of FRH and related constructs. The characterization of FRH helicase activity has the potential to be completed with various RNA substrates by following the protocols laid out in this work. Overall, FRH is a unique Mtr4-like helicase with roles in two essential biological pathways in *N. crassa (Guo et al., 2009)*. The potential impact of understanding FRH interactions can further both the knowledge of RNA surveillance and circadian oscillation pathways. Only further analysis of this intriguing RNA helicase will answer how FRH has linked the circadian oscillation and RNA surveillance pathways of *N. crassa*. The proposed work with the archless FRH construct, continued helicase assays, and the pursuit of FRH complex crystal structures will help to answer how FRH links circadian oscillation and RNA surveillance. The presented study of the unique RNA helicase FRH provides a foundation for future efforts to address the biological significance of the FRH dimer, to characterize the helicase activity of FRH, and to determine the similarities and differences between FRH and other Ski2-like helicases.

REFERENCES

Allmang, C., Kufel, J., Chanfreau, G., Mitchell, P., Petfalski, E., and Tollervey, D. (1999). Functions of the exosome in rRNA, snoRNA and snRNA synthesis. The EMBO Journal *18*, 5399–5410.

Altschul, S.F., Madden, T.L., Schaffer, A.A., Zhang, J., Zhang, Z., Miller, W., and Lipman, D.J. (1997). Gapped BLAST and PSI-BLAST: a new generation of protein database search programs. Nucleic Acids Res *25*, 3389-3402.

Aronson, B.D., Johnson, K.A., Loros, J.J., and Dunlap, J.C. (1994). Negative feedback defining a circadian clock: Autoregulation of the clock gene frequency. Science *263*, 1578-1584.

Baskaran, K., Duarte, J.M., Biyani, N., Bliven, S., and Capitani, G. (2014). A PDB-wide, evolution-based assessment of protein-protein interfaces. BMC Structural Biology *14*.

Berke, I.C., and Modis, Y. (2012). MDA5 cooperatively forms dimers and ATP-sensitive filaments upon binding double-stranded RNA. The EMBO Journal *31*, 1714–1726.

Bernstein, J., Patterson, D.N., Wilson, G.M., and Toth, E.A. (2008). Characterization of the Essential Activities of Saccharomyces cerevisiae Mtr4p, a 3' to 5' Helicase Partner of the Nuclear Exosome. Journal of Biological Chemistry *283*, 4930-4942.

Bernstein, J., and Toth, E.A. (2012). Yeast nuclear RNA processing. World Journal of Biological Chemistry *3*, 7-26.

Buttner, K., Nehring, S., and Hopfner, K. (2007). Structural basis for DNA duplex separation by a superfamily-2 helicase. Nature Structure & Molecular Biology *14*, 647 - 652.

Cheng, P., He, Q., Wang, L., and Liu, Y. (2005). Regulation of the Neurospora circadian clock by an RNA helicase. Genes & Development *19*, 234-241.

Chlebowskia, A., Lubasa, M., Jensenc, T.H., and Dziembowski, A. (2013). RNA decay machines: The exosome. Biochimica et Biophysica Acta (BBA) - Gene Regulatory Mechanisms *1829*, 552-560.

Cristodero, M., Bottcher, B., Diepholz, M., Scheffzek, K., and Clayton, C. (2008). The Leishmania tarentolae exosome: purification and structural analysis by electron microscopy. Molecular Biochem *159*, 24-29.

Duarte, J.M., Srebniak, A., Schärer, M.A., and Capitani, G. (2012). Protein interface classification by evolutionary analysis. BMC Bioinformatics *13*, 334.

Dunlap, J.C., and Loros, J.J. (2004). The Neurospora circadian system. Journal of Biological Rhythms *19*, 414–424.

Fabre, A., and Badens, C. (2014). Human Mendelian diseases related to abnormalities of the RNA exosome or its cofactors. Intractable Rare Dis Res *3*, 8-11.

Fairman-Williams, M.E., Guenther, U.P., and Jankowsky, E. (2010). SF1 and SF2 helicases: family matters. Curr Opin Struct Biol *20*, 313-324.

Falk, S., Weir, J.R., Hentschel, J., Reichelt, P., Bonneau, F., and Conti, E. (2014). The molecular architecture of the TRAMP complex reveals the organization and interplay of its two catalytic activities. Mol Cell *55*, 856-867.

Froehlich, A.C., Loros, J.J., and Dunlap, J.C. (2003). Rhythmic binding of a WHITE COLLAR-containing complex to the frequency promoter is inhibited by FREQUENCY. Proceedings of the National Academy of Sciences *100*, 5914-5919.

Guo, J., Cheng, P., and Liu, Y. (2010). Functional Significance of FRH in Regulating the Phosphorylation and Stability of Neurospora Circadian Clock Protein FRQ. Journal of Biological Chemistry *285*, 11508–11515.

Guo, J., Cheng, P., Yuan, H., and Liu, Y. (2009). The exosome regulates circadian gene expression in a posttranscriptional negative feedback loop. Cell *138*, 1236–1246.

Heintzen, C., and Liu, Y. (2007). The Neurospora crassa circadian clock. Advances in Genetics *58*, 25-66.

Hurley, J., Loros, J.J., and Dunlap, J.C. (2015). Dissecting the Mechanisms of the Clock in Neurospora. Methods in Enzymology *551*, 29-52.

Hurley, J.M., Larrondo, L.F., Loros, J.J., and Dunlap, J.C. (2013). Conserved RNA Helicase FRH Acts Nonenzymatically to Support the Intrinsically Disordered Neurospora Clock Protein FRQ. Molecular Cell *52*, 832–843.

Jackson, R.N., Klauer, A.A., Hintze, B.J., Robinson, H., Van Hoof, A., and Johnson, S.J. (2010). The crystal structure of Mtr4 reveals a novel arch domain required for rRNA processing. The EMBO Journal *29*, 2205-2216.

Jacobs Anderson, J.S., and Parker, R. (1998). The 3′ to 5′ degradation of yeast mRNAs is a general mechanism for mRNA turnover that requires the SKI2 DEVH box protein and 3′ to 5′ exonucleases of the exosome complex. The EMBO Journal *17*, 1497-1506.

Johnson, S.J., and Jackson, R.N. (2013). Ski2-like RNA Helicase Structures: Common Themes and Complex Assemblies. RNA Biology *10*, 33-43.

Jones, D. (1999). Protein secondary structure prediction based on position-specific scoring matrices. Journal of Molecular Biology *292*, 195-202.

Kantardjieff, K.A., and Rupp, B. (2003). Matthews coefficient probabilities: Improved estimates for unit cell contents of proteins, DNA, and protein-nucleic acid complex crystals. Protein Science *12*, 1865–1871.

Krissinel, E., and Henrick, K. (2007). Inference of macromolecular assemblies from crystalline state. Journal of Molecular Biology *372*.

Lauinger, L., Diernfellner, A., Faulk, S., and Brunner, M. (2014). The RNA helicase FRH is an ATP-dependent regulator of CK1a in the circadian clock of Neurospora crassa. Nature Communications *5*.

Liang, S., Hitomi, M., Hu, Y.H., Liu, Y., and Tartakoff, A.M. (1996). A DEAD-Box-Family Protein Is Required for Nucleocytoplasmic Transport of Yeast mRNA. Molecular and Cellular Biology *16*, 5139-5146.

Liu, Q., Greimann, J., and Lima, C. (2006). Reconstitution, Activities, and Structure of the Eukaryotic RNA Exosome. Cell *127*, 1223–1237.

Liu, Y., and Bell-Pedersen, D. (2006). Circadian rhythms in Neurospora crassa and other filamentous fungi. Eukaryotic Cell *5*, 1184-1193

Liu, Y., He, Q., and Cheng, P. (2003). Photoreception in Neurospora: A tale of two White Collar proteins. Cellular and Molecular Life Sciences *60*, 2131–2138.

Mitchell, P. (2014). Exosome substrate targeting: the long and short of it. Biochemical Society Transactions *42*, 1129-1134.

Mitchell, P., Petfalski, E., Shevchenko, A., and Mann, M. (1997). The exosome: a conserved eukaryotic RNA processing complex containing multiple 3′→5′ exoribonucleases. Cell *91*, 457–466.

Otwinowski, Z., and Minor, W. (1997). Processing of X-ray Diffraction Data Collected in Oscillation Method, Macromolecular Crystallography. Methods in Enzymology *276*, 307-326.

Rudolph, M.G., and Klostermeier, D. (2009). The Thermus thermophilus DEAD box helicase Hera contains a modified RNA recognition motif domain loosely connected to the helicase core. RNA *15*, 1993-2001.

Schneider, C., and Tollervey, D. (2013). Threading the barrel of the RNA exosome. Trends in Biochemical Sciences *38*, 485–493.

Shi, M., Collett, M., Loros, J.J., and Dunlap, J.C. (2010). FRQ-Interacting RNA Helicase Mediates Negative and Positive Feedback in the Neurospora Circadian Clock. Genetics *184*, 351-361

Story, R.M., Li, H., and Abelson, J.N. (2001). Crystal structure of a DEAD box protein from the hyperthermophile Methanococcus jannaschii. Proc Natl Acad Sci U S A *98*, 1465-1470.

Taylor, L.L. (2014). Detailed Analysis of the Domains of Mtr4 and How They Regulate Helicase Activity. All Graduate Theses and Dissertations.

Taylor, L.L., Jackson, R.N., Rexhepaj, M., Klauer King, A., Lott, L.K., Van Hoof, A., and Johnson, S.J. (2014). The Mtr4 ratchet helix and arch domain both function to promote RNA unwinding. Nucleic Acids Research.

Thom, M., Thomson, E., Baβler, J., Gnadig, M., Griesel, S., and Hurt, E. (2015). The Exosome is Recruited to RNA Substrates through Specific Adaptor Proteins. Cell *162*, 1029-1038.

Vanacova, S., Wolf, J., Martin, G., Blank, D., Dettwiler, S., Friedlein, A., Langen, H., Keith, G., and Keller, W. (2005). A new yeast poly(A) polymerase complex involved in RNA quality control. PLoS Biol *3*, e189.

Viegas, S.C., Silva, I.J., Apura, P., Matos, R.G., and Arraiano, C.M. (2015). Surprises in the 3′-end: 'U' can decide too! FEBS *282*, 3489-3499.

Wang, H.-W., Wang, J., Ding, F., Callahan, K., Bratkowski, M.A., Butler, J.S., Nogales, E., and Ke, A. (2007). Architecture of the yeast Rrp44 exosome complex suggests routes of RNA recruitment for 3′ end processing. PNAS *104*, 16844–16849.

Wang, X., Jia, H., Jankowsky, E., and Anderson, J.T. (2008). Degradation of hypomodified tRNA(iMet) in vivo involves RNA-dependent ATPase activity of the DExH helicase Mtr4p. RNA *14*, 107-116.

Weichenberger, C., and Rupp, B. (2014). Ten years of probabilitic estimates of biocrystal solven content: New insights via nonparamatric kernel density estimate. Acta Crystallography *70*, 1579-1588.

Weir, J.R., Bonneau, F., Hentschel, J., and Conti, E. (2010). Structural analysis reveals the characteristic features of Mtr4, a DExH helicase involved in nuclear RNA processing and surveillance. Proc Natl Acad Sci U S A *107*, 12139-12144.

Wyers, F., Rougemaille, M., Badis, G., Rousselle, J.C., Dufour, M.E., Boulay, J., Regnault, B., Devaux, F., Namane, A., Seraphin, B., *et al.* (2005). Cryptic pol II transcripts are degraded by a nuclear quality control pathway involving a new poly(A) polymerase. Cell *121*, 725-737.

Zhao, R., Shen, J., Green, M.R., MacMorris, M., and Blumenthal, T. (2004). Crystal structure of UAP56, a DExD/H-box protein involved in pre-mRNA splicing and mRNA export. Structure *12*, 1373-1381.

APPENDICES

APPENDIX A

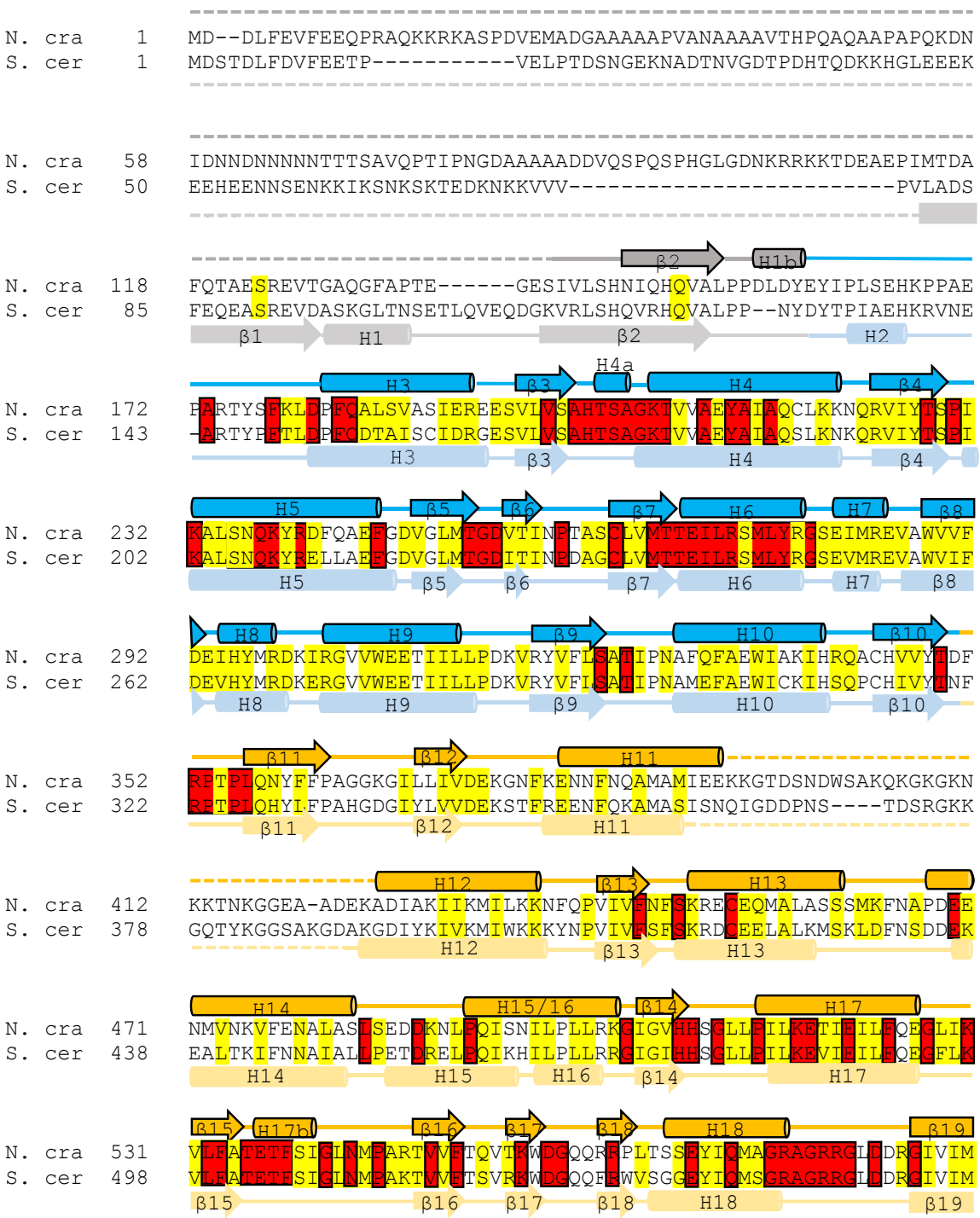
N. cra 1 MD--DLFEVFEEQPRAQKKRKASPDVEMADGAAAAAPVANAAAAVTHPQAQAAPAPQKDN
S. cer 1 MDSTDLFDVFEETP----------VELPTDSNGEKNADTNVGDTPDHTQDKKHGLEEEK
N. cra 58 IDNNDNNNNNTTTSAVQPTIPNGDAAAAADDVQSPQSPHGLGDNKRRKKTDEAEPIMTDA
S. cer 50 EEHEENNSENKKIKSNKSKTEDKNKKVVV----------PVLADS
β2
H1b
N. cra 118 FQTAESREVTGAQGFAPTE------GESIVLSHNIQHQVALPPDLDYEYIPLSEHKPPAE
S. cer 85 FEQEASREVDASKGLTNSETLQVEQDGKVRLSHQVRHQVALPP--NYDYTPIAEHKRVNE
β1
H1
β2
H2
H4a
H3
β3
H4
β4
N. cra 172 PARTYSFKLDPFQALSVASIEREESVLVSAHTSAGKTVVAEYAIAQCLKKNQRVIYTSPI
S. cer 143 -ARTYPFTLDPFQDTAISCIDRGESVLVSAHTSAGKTVVAEYAIAQSLKNKQRVIYTSPI
H3
β3
H4
β4
H5
β5
β6
β7
H6
H7
β8
N. cra 232 KALSNQKYRDFQAFFGDVGLMTGDVTINPTASCLVMTTEILRSMLYRGSEIMREVAWVVF
S. cer 202 KALSNQKYRELLAFFGDVGLMTGDITINPDAGCLVMTTEILRSMLYRGSEVMREVAWVIF
H5
β5
β6
β7
H6
H7
β8
H8
H9
β9
H10
β10
N. cra 292 DEIHYMRDKIRGVVWEETIILLPDKVRYVFLSATIPNAFQFAEWIAKIHRQACHVVYTDF
S. cer 262 DEVHYMRDKERGVVWEETIILLPDKVRYVFLSATIPNAMEFAEWICKIHSQPCHIVYTNF
H8
H9
β9
H10
β10
β11
β12
H11
N. cra 352 RPTPLQNYFFPAGGKGILLIVDEKGNFKENNFNQAMAMIEEKKGTDSNDWSAKQKGKGKN
S. cer 322 RPTPLQHYIFPAHGDGIYLVVDEKSTFREENFQKAMASISNQIGDDPNS----TDSRGKK
β11
β12
H11
H12
β13
H13
N. cra 412 KKTNKGGEA-ADEKADIAKIIKMILKKNFQPVIVFNFSKRECEQMALASSSMKFNAPDEE
S. cer 378 GQTYKGGSAKGDAKGDIYKIVKMIWKKKYNPVIVFSFSKRDCEELALKMSKLDFNSDDEK
H12
β13
H13
H14
H15/16
β14
H17
N. cra 471 NMVNKVFENALASLSEDQKNLPQISNILPLLRKGIGVHHSGLLPILKETIEILFQEGLIK
S. cer 438 EALTKIFNNAIALLPETDRELPQIKHILPLLRRGIGIHHSGLLPILKEVIEILFQEGFLK
H14
H15
H16
β14
H17
β15
H17b
β16
β17
β18
H18
β19
N. cra 531 VLFATETFSIGLNMPARTVVFTQVTKWDGQQRRPLTSSEYIQMAGRAGRRGLDDRGIVIM
S. cer 498 VLFATETFSIGLNMPAKTVVFTSVRKWDGQQFRWVSGGEYIQMSGRAGRRGLDDRGIVIM
β15
β16
β17
β18
H18
β19

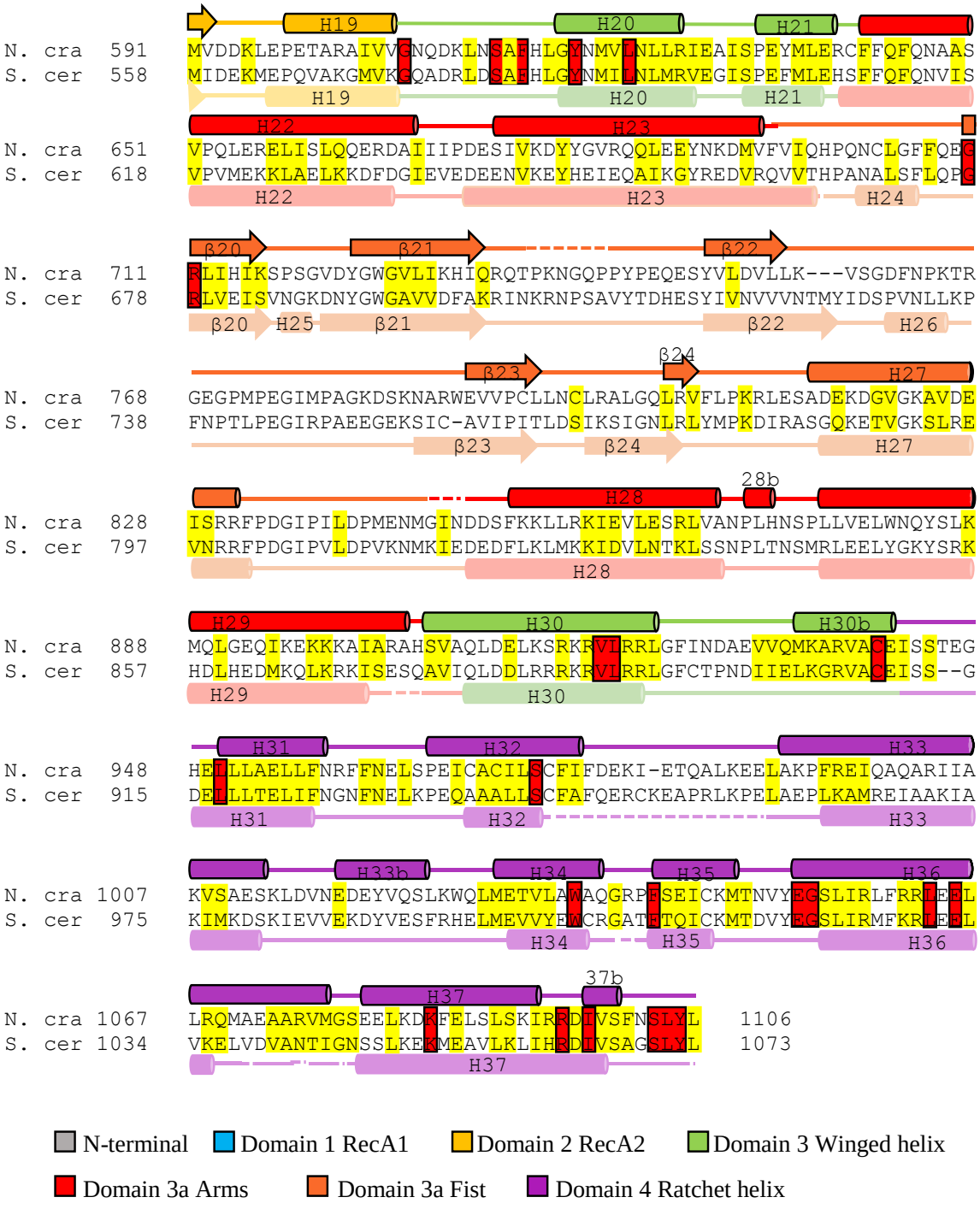

Appendix Figure A1. Secondary Structure Alignment of FRH and scMtr4. Neurospora crassa (N. cra) FRH primary sequence is aligned to the Saccharomyces cerevisiae (S. cer) sequence of scMtr4. Secondary structure is depicted for helices (cylinders), beta-sheets (arrows), and random coils (lines) from the solved FRH structure and scMtr4 (PDB ID: 4QU4) with unbuilt regions

indicated (dashed lines). Helices and beta sheets are numbered according to the scMtr4 structure for comparison. Sequence conservation for eleven species of Mtr4 and eight species of Ski2 helicases is indicated for strictly conserved residues (red) and similar residues (yellow) as published in Jackson *et al*. 2010.

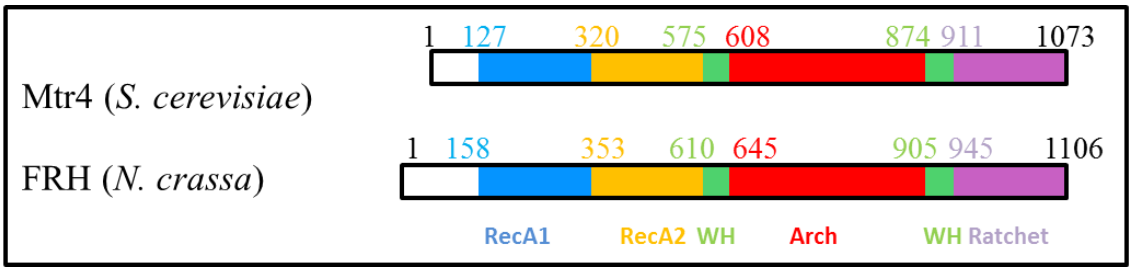

Figure A2. Domain alignments of scMtr4 and FRH. scMtr4 (top) is 1073 amino acids long while FRH (bottom) is 1106 amino acids in length. The core domains are all present in FRH based on alignment with the scMtr4 sequence with RecA1(blue), RecA2 (yellow), Winged helix (green), Arch (red), and Ratchet helix (purple). The two N-termini (white) are different in length and do not align well. Residue numbers are indicated for the beging and end of the sequences as well as the start of each domain.

Table A1. Domain Definition for FRH and scMtr4

Domain	FRH Residues	scMtr4 Residues
N-terminal	1-157	1-126
Domain 1	158-352	127-319
Domain 2	353-609	320-574
Domain 3	610-644, 905-944	575-607, 874-910
Domain 3a	645-904	608-873
Arms	645-697, 855-904	607-664, 818-873
Fist	698-854	665-817
Domain 4	945-1106	911-1073

Table A2. Sequence Identity and Similarity for FRH and scMtr4 domains

Region	Sequence Identity (%)	Sequence Similarity (%)
N-terminal	40%	60%
Domain 1	81%	87%
Domain 2	63%	77%
Domain 3 before arch	77%	96%
Domain 3a	39%	62%
Arms ascending	42%	69%
Fist	37%	59%
Arms descending	44%	68%
Domain 3 after arch	58%	80%
Domain 4	51%	69%
Total	57%	73%

Pairwise alignment comparing scMtr4 and FRH with identity and similarity of sequences calculated using NCBI protein BLAST

Table A3. RMS Values of Domains

Domain	RMS align	Cα Atoms	RMS current	Cα Atoms
Domain 1	0.535	157	2.84	188
Domain 2	0.955	187	1.618	224
Domain 3	0.946	53	2.214	72
Arch arms	2.750	98	3.167	104
Arch fist	1.507	113	2.943	147
Domain 4	1.236	104	3.14	143

RMS values calculated in PyMol using the align command which aligns two selections and calculates a refined RMS value for the c-alpha carbons. The RMS_cur command was then used to compare all of the c-alpha atoms in the previously performed alignment. The c-alpha atoms for each calculation are included.

APPENDIX B

Jacqueline Johnson

Department of Chemistry and Biochemistry

Utah State University, Logan, UT 84322-3900

Cell Phone: (208)-749-9031

Email: Jacqueline.johnson@aggiemail.usu.edu

EDUCATION

M.S., Biochemistry	May 2016
Utah State University, Logan, Utah, USA	GPA 3.80
B.S., Biochemistry	May 2013
Washington State University, Pullman, Washington, USA	GPA 3.42

CERTIFICATIONS

- Lab Safety Training, Utah State University Aug. 2013
- Radiation Safety Training, Utah State University Sept. 2013

RESEARCH EXPERIENCE

- **Graduate Research Assistant**
  Department of Biochemistry, Utah State University 2013-Present
  - Developing purification protocols for proteins of unknown structure, performing activity assays, and structurally analyzing proteins through X-ray diffraction
- **Undergraduate Research Assistant**
  Department of Chemistry, Washington State University 2012-2013
  - Worked with HPLC to analyze prostate specific membrane antigen activity with various inhibitors, used aseptic cell culture techniques and protein purification

TEACHING EXPERIENCE

Teaching Assistant

Utah State University, Logan UT August 2013-Spring 2015

CHEM1215-Introduction to Chemistry Lab Fall 2013, 2014

- Assisted students in lab, graded student assignments, and assigned final grades

CHEM 5720- Advanced Biochemistry Lab Spring 2014, 2015

- Prepared lab materials, graded student reports, discussed biochemical concepts, and enhanced the understanding of biochemistry

CHEM 3710- Introductory Biochemistry Lab Spring 2016

- Introduced students to biochemistry concepts through simple experiments

Tutor

Utah State University- Disability Resources Center Fall 2014-Present

- Assisted blind student in chemistry study (CHEM 1210, 1220, 2300, & 3700)

Utah State University- Chemistry Department 2013-2014

- Lead students in general chemistry and biochemistry topics

Washington State University-

Multicultural Student Center, Pullman, WA 2011-2012

- Helped students with general biology and general chemistry studying

WORK EXPERIENCE

Internships

Richard J. Lee Group Inc., Pasco Washington Lab Tech. Summer 2011

- Simulated sludge mixing project

Washington River Protection Solutions Summer 2010

- Prepared environmental awareness documentations

PUBLICATIONS

Lisa Y. Wu, **Jacqueline M. Johnson**, Jessica K. Simmons, Desiree E. Mendes, Jonathan J. Geruntho, Tiancheng Liu, Wessel P. Dirksen, Thomas J. Rosol, William C. Davis, and Clifford E. Berkman. *Biochemical Characterization of Prostate-Specific*

Membrane Anitgen from Canine Prostate Carcinoma Cells. Prostate. 74(5):451-7 DOI: 10.1002/pros.22727. May 2014.

Tiancheng Liu, Lisa Y. Wu, Melody D. Fulton, **Jacqueline M. Johnson**, and Clifford E. Berkman. *Prolonged androgen deprivation leads to downregulation of androgen receptor and prostate-specific membrane antigen in prostate cancer cells*. International Journal of Oncology. 41(6):2087-92 DOI: 10.3892/ijo.2012.1649. December 2012.

AWARDS AND HONORS

- SACNAS National Conference Travel Scholarship 2014, 2015
- USU School of Graduate Studies Travel Award, 2015
- Piette Scholarship, Utah State University, 2014
- Hansen Graduate Fellowship, Utah State University, 2013
- USU Chemistry and Biochemistry Departmental Fellowship, 2013
- Washington State University Biology Summer Grant, 2012
- Washington State University Deans list, 2010-2011
- Washington State University Academic Scholarship 2009-2011
- Girl Scouts of America, Gold Award, 2009

LEADERSHIP

- Society for Advancement of Hispanics/Chicanos and Native Americans in Science (SACNAS) USU Chapter member, Fall 2014-present
- SACNAS USU Chapter, President, Fall 2015-present
- Washington State University Microbiology Club Secretary, Fall 2012-Spring 2013
- Girl Scouts of America Lifetime member, 2009-present

PRESENTATIONS AT PROFESSIONAL MEETINGS

Posters

Johnson, Jacqueline, Sean Johnson, "Structural Characterization of the Frequency-interacting RNA Helicase from *Neurospora crassa*". FASEB Helicase Conference, summer 2015, Steamboat Springs, CO.

Johnson, Jacqueline, Sean Johnson, "Initial Biochemical & Structural Characterization of the Frequency-interacting RNA Helicase, an Mtr4 Homolog". USU Research Symposium, spring 2015, Logan, UT

Johnson, Jacqueline, Sean Johnson, "Purification and Initial Structural Characterization of Frequency-interacting RNA Helicase, an Mtr4-like Protein". USU, Hansen Retreat, fall 2014, Logan, UT

Johnson, Jacqueline, Sean Johnson, "Initial Biochemical and Structural Studies of Frequency-Interacting RNA Helicase, an Mtr4-like Protein from *Neurospora crassa*". USU Research Symposium, spring 2014, Logan, UT

Johnson, Jacqueline, Lisa Y. Wu, and Clifford E. Berkman, "Canine Carcinoma Cells Containing Prostate-Specific Membrane Antigen". WSU Spring 2013, Pullman, WA.

PROFESSIONAL RETREATS AND CONFERENCES

- SACNAS National Conference, Washington D.C. Oct. 2015
- FASEB Helicase Conference, Steamboat Springs, CO July 26-31, 2015
- SACNAS National Conference, Los Angeles, CA Oct. 2014
- Hansen Life-Sciences Retreat Sept. 2013, 2014, 2015
- Getting Started as a Successful Proposal Writer and Academician Feb. 2014

SERVICE ACTIVITIES

- Science Unwrapped demonstrator September 2014-Present